Evaluating the Effect of Neck Strength on Concussions

-MQP Report-

Submitted To:

Project Advisor: Brian J. Savilonis, WPI Professor

Submitted By:

Karly Bigham

Abigail Gilbert

Thomas Hanlon

Mitchell Holman

Date: 7 April 2020

Abstract

The goal of this MQP was to create a neck and head test fixture to assess the relationship between neck strength and concussion prevalence. The fixture was created primarily out of steel and consisted of a tensioning cable through alternating rubber and aluminum disks which was tensioned to simulate various neck strengths. Concussive impacts were induced using a 9 ft tall pendulum and various weights were used to change the force of impact. Data was collected using an Arduino and two AXDL 377 accelerometers placed inside the head of the fixture. Microsoft Excel was then used to convert the raw acceleration data to an HIC value, a common metric used for predicting concussion likelihood. HIC values were compared across varying neck strengths to determine the correlation between neck strength and concussions. By conducting 70 trials using the concussion fixture, we found that HIC values are 5.9 percent higher for females than males when subjected to the same impact.

Acknowledgements

We would like to thank the individuals that contributed to our project's findings and success. First, we would like to thank our project advisor, Professor Savilonis for providing consistent support and guidance throughout the duration of our project. In addition, Professor Sabuncu and WPI student Eric Hall, for providing data acquisition assistance and help with Arduino programming. We would also like to thank Professor Songbai Ji for his consultation on a material to simulate the brain. This project would not have been successful without the continuous guidance from Ian Anderson and James Loiselle in WPI's machine shop to assist with the construction of our fixture. Finally, we would like to thank St. Pierre Wire Rope for their expertise and for donating the steel tensioning cable used in our fixture.

Table of Contents

List of Figures

List of Tables

1. Introduction

Between 1.7 and 3 million concussions are diagnosed each year during sports and recreation, with an estimated 50 percent of all concussions remaining undetected (UPMC, 2019). A concussion is a form of mild traumatic brain injury (MTBI) caused by a direct blow to the head or body that results in a temporary decrease in neurological function (Chancellor et al., 2019). The rapid back and forth motion of the brain causes stress to the cerebral tissue which results in an altered mental state. Concussions can be caused by both linear acceleration and rotational acceleration of the head. Linear acceleration of the head can induce concussive pressure waves throughout the brain, whereas rotational acceleration can result in concussive shear strain in the brain (Chancellor et al., 2019) Symptoms of concussions include, but are not limited to, dizziness, headaches, fatigue, difficulty concentrating, and loss of balance (Littleton & Guskiewicz, 2013).

Certain risk factors such as age and gender have been shown to impact concussion likelihood. One study showed that concussions are most likely to occur in adolescents. In fact, the study showed that 32% of diagnosed concussions occur between the age of 10 to 19 years (Zhang et al., 2016). In addition, females have been shown to be more likely to sustain concussions and are up to 2.6 times more likely to be diagnosed with a concussion than male athletes (Caccese et al., 2017). One hypothesized reason for this is the variation in neck strength between males and females. One study showed that neck strength is an important factor in reducing total rotational accelerations of the head (Daneshvar et al., 2011). Research on the relationship between neck strength and concussion risk is limited, leaving significant room for exploration.

This project aimed to create a concussion test fixture which accurately models the relative mechanical properties of the human neck, in order to evaluate the relationship between human neck strength and concussion prevalence. To achieve our goal, we had the following objectives: (1) Design a test fixture which accurately simulates the relative properties of the human neck and head, (2) Use CAD simulations to determine that the fixture will withstand the force of impact, (3) Test the completed fixture to confirm it accurately models the relative mechanical properties of a human neck, (4) Assess the relationship between neck strength and concussion likelihood. To achieve these objectives, we conducted material research and leveraged an existing neck design from previous research. We used SolidWorks to design the fixture and run stress simulations to ensure that the materials we used would sustain the forces it was exposed to during testing. Once the fixture was designed and assembled, we tested the fixture to ensure that it properly represented the mechanical properties of the human head and neck, while allowing for adjustable neck strength. Finally, we used a pendulum test rig to test our hypothesis that weak necks would be more likely to sustain concussions than strong necks. Assessing the impact between human neck strength and concussion risks can further research in the field of concussions.

2. Background

Sports induced concussions are becoming more frequently reported among athletes (Littleton & Guskiewicz, 2013). The improper management of concussions can lead to subsequent cognitive risks, causing permanent brain damage. In this chapter, we evaluate the criteria for a concussion and characteristics that affect concussion prevalence among individuals. We also identify current test methods and fixtures as well as the materials that have been used to model the head, neck, and brain.

2.1 Evaluating Concussions

Understanding the criteria and impact strength necessary for a concussion to occur is important for engineers to understand when designing test fixtures. In this section, we describe the most widely accepted numerical metric for evaluating concussions as well as the impact forces likely to induce a concussion. We also describe the different types of head accelerations and the impacts that cause them.

2.1.1 Types of Impacts

There are different types of impact that can affect the likelihood of a concussion. The main factor differentiating one impact from another is the location of the impact. The location of impacts can be characterized as top-of-the-head impacts (exceeding 65 degrees of elevation from the horizontal plane through the head's center of gravity), front impacts (within 45 degrees of the sagittal plane anteriorly), back impacts (within 45 degrees of the sagittal plane posteriorly), or side impacts (within 45 degrees of the frontal plane on either side). Studies have shown that impacts from the front or top of the head have higher risk of causing concussions (Liao et al., 2016). Impacts to the front of the head can simultaneously twist and accelerate the

head, and the combination of the two increase the likelihood of traumatic brain injury (Pellman et al., 2003).

While direct impacts to the head are known for causing concussions, whiplash may also cause traumatic brain injury (Youmans, 2018). Whiplash can be caused by a direct hit to the body, causing the head and neck to jerk quickly. Studies have shown that the activation of neck muscles can decrease the acceleration of the head, reducing the risk of a concussion. Neck muscles are not able to activate quickly enough when a person is subject to a concussive impact or a hit causing whiplash (Wood et al., 2019).

2.1.2 Forces Causing Concussions

When the body or head experiences an impact there is an acceleration of the head. During these impacts the brain and the skull accelerate at different speeds causing a relative motion between the brain-skull interface. This motion leads to strains and pressures in the brain. The forces associated with impacts vary with different sports. An analysis of video footage in professional football found that concussions occurred in impacts that had accelerations of 98 ± 28 g and 6432 ± 1813 rad/s^2. In soccer the main cause of concussions is head to head impact. An analysis of FIFA soccer matches where there was head to head impacts saw average forces of 87g and 7033 rad/s^2. Baseball has even lower accelerations ranging from 26 to 42g and 1974 to 5266 rad/s^2 for ball to mask impacts for catchers. While the accelerations caused by impacts in these sports are lower than football, evidence suggests that these accelerations may still cause concussions (Rowson et al., 2016).

2.1.3 Linear vs. Angular Accelerations

In contrast to focal brain injuries that are caused from a direct hit effecting the cerebral fluid and vessels, a diffuse injury is typically less severe and is caused by a sudden acceleration or deceleration of the head (Littleton & Guskiewicz, 2013). This sudden change in acceleration can be due to a linear impact, rotational impact or a combination of both. There are many mathematical metrics, such as the ones we explain is sections 2.1.4 and 2.1.5, to predict the severity of translational accelerations caused by linear impacts, however, until recently, angular accelerations were not considered (Nazarian et al., 2015). Today, scientists now know that concussions can be caused by purely rotational accelerations, which is the movement about the vertical axis and can be caused by impacts that may or may not be directly to the head.

Rotational accelerations can occur when other parts of the body are hit and cause the brain to jolt one way or the other causing a whiplash effect (Youmans, 2018). When the head experiences a quick, rotational acceleration where the brain tissue exceeds its critical strain value, injuries such as subdural hematomas or diffuse axonal injury may occur (Nazarian et al., 2015). In contrast, when a head is hit directly and linearly accelerates, the brain collides with the skull and immediately decelerates. Depending on the force of the hit, this internal collision may cause a concussion.

2.1.4 Head Injury Criterion

There are a variety of different injury indices which use numerical data to determine the likelihood of concussions. The Head Injury Criterion (HIC) is the most widely used of all concussion metrics. The HIC equation assesses the time-averaged acceleration within a given time interval. The equation for HIC is defined below:

$$HIC = \max_{t_1, t_2} \left\{ \left[\frac{1}{t_2 - t_1} \int_{t_1}^{t_2} a(t)dt \right]^{2.5} (t_2 - t_1) \right\}$$

In this equation, t_1 and t_2 represent the initial and final times (measured in seconds) that will result in the maximum HIC value, and the acceleration (a) is normalized with respect to gravitational acceleration (g). The time duration is typically constrained to a maximum of 15ms, since concussive blows rarely occur over a larger time interval (Nazarian et al., 2015). In a biomechanics study conducted at Wayne State University, it was determined that a concussion is likely to occur in most athletes when HIC $\geq$ 250 (Viano, 2005).

2.1.5 Head Impact Power

Another relevant injury index is the Head Impact Power (HIP). Unlike the HIC which considers only translational acceleration, HIP includes both linear and angular components. Since concussions have been shown to be caused by both linear and angular acceleration of the head, this metric is valuable in concussion research. The equation for HIP is shown as follows:

$$HIP = \underbrace{C_1 a_x \int a_x dt + C_2 a_y \int a_y dt + C_3 a_z \int a_z dt}_{Linear\ contribution} + \underbrace{C_4 \alpha_x \int \alpha_x dt + C_5 \alpha_y \int \alpha_y dt + C_6 \alpha_z \int \alpha_z dt}_{Angular\ contribution}$$

In this equation, $C_1 = C_2 = C_3$ are equal to the mass of the head being tested; C_4, C_5 and C_6 are equal to the moments of inertia of the head about the x, y and z axes, respectively. The linear accelerations of the head are recorded as a_x, a_y and a_z and the angular accelerations of the head are α_x, α_y and α_z. Because the HIP equation is time dependent, the time instance with the largest resultant HIP value is chosen (Marjoux et al., 2006).

2.2 Factors Affecting Concussion Prevalence

In order to properly design a concussion test fixture, especially a fixture capable of representing a variety of different neck strengths, it is important to understand the various parameters that affect concussion prevalence. In the following section, we address the impact of age, gender and neck strength on concussion probability.

2.2.1 Age

Age is one factor that affects the likelihood of a concussion occurring. One study conducted at the University of California – San Francisco used the health records from over 8 million patients to assess concussion incidences based on age. The study showed that 32% of the diagnosed concussions occurred from patients of ages 10 to 19 years (Zhang et al., 2016). Not only are adolescents more likely to compete in concussion-causing sporting events than other age groups, but nerve connections in the brain are also not yet fully developed, which further increases concussion risk (Rowson et al., 2016).

2.2.2 Gender

Along with age, gender is another important factor that impacts concussion likelihood. There is significant evidence that in sports with similar rules for different genders, females are more likely to sustain a concussion than males (Littleton & Guskiewicz, 2013). In fact, female athletes are up to 2.6 times more likely to be diagnosed with a concussion than male athletes. In one study, male and female soccer athletes completed controlled soccer headers with the same initial ball velocity. The study showed that linear and angular acceleration of the female heads (40.9 ± 13.3 g; 3279 ± 1065 rad/s^2) were significantly higher than the males (27.6 ± 8.5 g, 2219 ± 823 rad/s^2). This information indicates that under a controlled impact, females are likely

to have head acceleration values approximately 1.5 times greater than males (Caccese et al., 2017). While there has been ongoing debate on the reason behind the increased concussion prevalence in females, this study may suggest that a biomechanical factor, such as the reduced neck strength of females, may be the cause (Rowson et al., 2016). Among other hypotheses is that differences in neuromuscular control and spine kinematics of females increases concussion probability (Littleton & Guskiewicz, 2013).

Another study was conducted in order to find the passive stiffness of the human neck for males and females (McGill et al., 1994). Torques were applied to the subjects' heads in order to determine the bending moments and stiffness of their necks. The stiffness was calculated using the resulting angles of the neck when subjected to specific torques. These tests were done in extension, tension, and lateral bending defined in Figure 1. The results of the study can be found in Table 1 below.

Table 1: Male vs. Female Bending Moment and Passive Neck Stiffness (McGill et al., 1994)

	Angle (degrees)	Bending moment (N m)		Stiffness (N m/degrees)	
		Male	Female	Male	Female
Extension	10	0.6	0.2	0.03	0.01
	20	1.0	0.4	0.05	0.02
	30	1.6	0.7	0.07	0.04
	40	2.5	1.2	0.12	0.08
	50	4.0	2.3	0.19	0.14
	60	6.4	4.3	0.30	0.26
Flexion	10	1.2	1.0	0.05	0.04
	20	1.9	1.4	0.08	0.06
	30	2.8	2.1	0.12	0.08
	40	4.3	3.2	0.17	0.13
	50	6.4	4.8	0.26	0.19
Right lat. bend	10	0.8	0.5	0.05	0.03
	20	1.5	0.8	0.09	0.04
	30	2.7	1.4	0.16	0.08
	40	4.9	2.4	0.29	0.19
Left lat. bend	10	0.9	0.5	0.05	0.03
	20	1.6	0.9	0.09	0.05
	30	2.9	1.6	0.17	0.10
	40	5.2	3.1	0.31	0.20
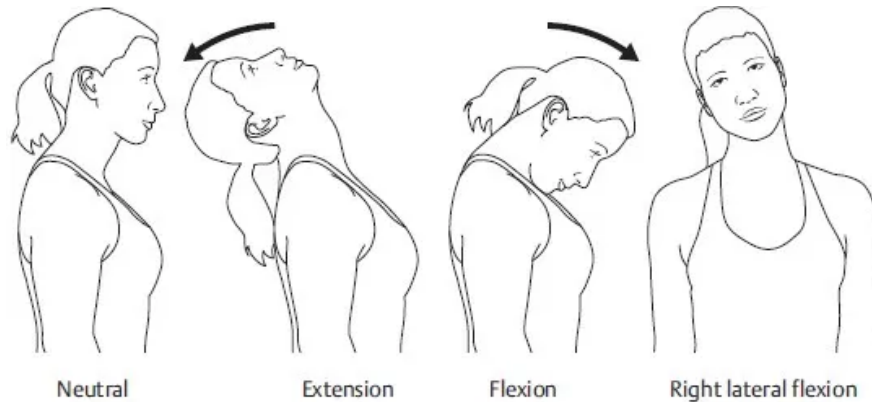
Figure 1: Defining Bending Movements of the Neck

The stiffness values for the males were higher than the females in every category. Looking specifically at the stiffness for extension at 10 degrees, the male stiffness of 0.03 Nm/deg is 3 times stiffer than the female neck at 0.01 Nm/deg. In addition, it seems male necks are approximately 1.5 times as stiff as female necks when bent laterally at 50 degrees. In contrast, when extended at 50 degrees, male necks are only about 1.3 times as stiff. This suggests that male and female necks may differ more when subject to a lateral bending test than in extension, and that hits resulting in a lateral movement have a higher impact on females than males. The data from this study shows that there is clearly a difference between the anatomy of male and female necks that could possibly correlate to a difference in concussion prevalence.

2.2.3 Neck Strength

Another parameter that may have a significant impact on concussion risk is overall neck strength. A research study by Collins et al. (2014) evaluated the impact of neck strength on concussion prevalence in 6,662 athletes. The active neck strength was evaluated using hand-held tension scales and dynamometers. When the data was compared with the subjects' genders,

sports, and concussion history, it was found that concussion risk decreased by 5 percent for every one-pound increase in neck strength. One limitation to this study is that it only measured the active neck strength of an individual. During a blind hit, an individual may not have time to activate their neck muscles. Another study that involved the biomechanical reconstruction of concussive impacts on NFL athletes highlighted the role of rotational acceleration of the head in concussion risk. The study indicated that neck strength is an important factor in reducing concussive rotational accelerations (Daneshvar et al., 2011).

2.3 Properties of the Neck

We must research the characteristics of the human neck in order to accurately replicate and test it in our model. In this section, we discuss the mechanical properties of the human neck which will become important during construction and testing.

A study conducted by Catenaccio et al. (2017) found that neck strength in young adults varies greatly (Table 2). The testing was performed using a fixed frame dynamometry and measured strength in the four main directions. Three trials were completed with each direction and they were given a 5 second rest between trial and 30 second rest between direction. The dynamometer was pushed against and recorded the peak force exerted. The weight, mass index, and neck circumference were only moderately correlated with neck strength. Males however had greater neck strength in general compared to women with an average neck strength range of 37-377 N for males and 15-215 N for females. The study calculated the percentile values for average neck strength across 3 trials. Males had significantly stronger necks in extension, forward flexion, right flexion and left flexion. For both extension and forward flexion of the 50th percentile, male necks were around 1.6 times stronger than female necks (Catenaccio et al., 2017).

Table 2: Neck Strength for Males and Females in Newtons (Catenaccio et al., 2017)

	Direction	5th	10th	25th	50th	75th	90th	95th
Men	Extension	104.0	118.4	162.8	210.6	250.5	292.2	314.3
	Forward flexion	73.0	92.6	113.2	136.2	165.5	183.5	194.8
	Right lateral flexion	59.3	66.2	83.0	121.6	161.4	199.4	217.8
	Left lateral flexion	58.0	68.1	91.7	119.6	159.9	194.0	217.6
Women	Extension	58.7	80.7	105.9	127.6	160.6	179.0	185.6
	Forward flexion	51.0	58.7	70.0	83.2	97.8	110.2	113.9
	Right lateral flexion	40.0	49.2	64.1	83.1	95.1	108.1	118.1
	Left lateral flexion	39.8	50.4	63.8	76.8	96.7	106.1	114.2

2.4 Properties of the Head

Understanding the mechanical properties of the head is important for us to understand when designing our test fixture. In the following subsections, we identify the properties of the skull and the brain so that we can accurately select materials to model them in our fixture.

2.4.1 Skull Properties

The skull is formed of many different bones that fuse together in adulthood. The bones that makeup the skull have different layers. The middle layer of cranial bone, called diploe or spongey bone, is surrounded on either side by compact bone that is denser (Rice University, 2013). The structure of skull bone can be seen in Figure 2 below.
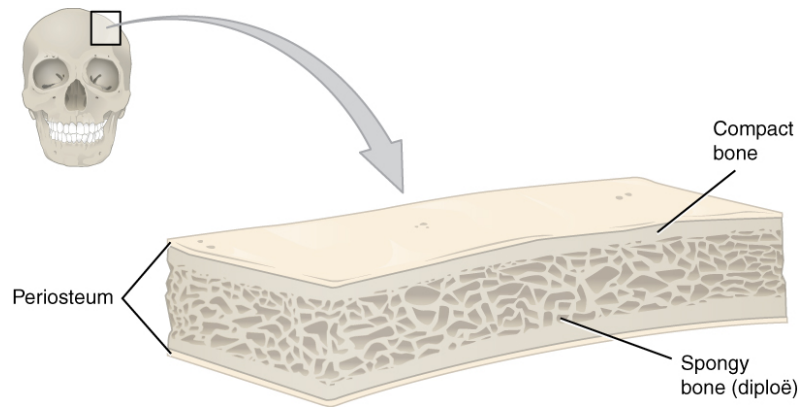
Figure 2: Skull Bone Anatomy

Determining the mechanical properties of skull bone is challenging because of its structure and the way it is formed. The different layers of bone that make up the skull can vary in strength, shear, and other properties. One of the first studies to calculate the mechanical properties of cranial bone was done in 1970. McElhaney et al. (1970) used cadaver skulls and performed various tests on different cross sections of cranial bone. A more recent study done by Motherway et al. in 2010 characterized the properties of cortical bone taken from different parts of the skull-- Left Parietal (LP), Right Parietal (RP), and Frontal (F)-- under different shear strain rates. This study found that mechanical properties vary under different speeds, strain rates, or cranial sampling positions. The values for some of the mechanical properties that this study found are shown in Table 3 (Motherway et al., 2010).

Table 3: Properties of Cranial Bone (Motherway et al., 2010)

Speed (m/s)	Position	Max Force (N)	E (GPa)	σ_{rupt} (MPa)	Strain Rate (s^{-1})
0.5	RP	735	10.3	84.5	21.1
1.0	RP	794	9.44	82.9	30.8
2.5	RP	1160	12.8	123	109
0.5	LP	722	5.70	82.1	20.9
1.0	LP	584	17.7	78.2	26.0
2.5	LP	1230	18.1	134	107
0.5	F	1060	4.35	90.8	21.8
1.0	F	1035.7	4.87	203	26.3
2.5	F	1315.9	16.3	127	104

Based on the table above, we conclude that the elastic modulus and rupture stress for cranial bone varies depending on the speed and strain rate of the impact. However, the elastic modulus remains in the range of ~4-18 GPa and the rupture stress can be estimated within the range of ~70-210 MPa.

2.4.2 Brain Properties

The brain floats in cerebrospinal fluid beneath the hard-outer skull that protects it (Bilston, 2011). Because it floats beneath the skull, it moves relative to the skull upon impact. It consists of both grey and white matter that differ in the type of neurons they are made from, their function, and their density. The different mechanical properties of these types of matter in the brain is part of what makes the brain so difficult to model (Johnson, 2014). Furthermore, there are various test methods and constitutive models of the brain, making the mechanical properties vary on orders of different magnitude (Van Dommelen et al., 2009). Understanding the mechanical properties of the brain helps researchers to accurately model the brain's response to impacts and complex loading conditions. These simulations allow scientists to better understand traumatic brain injury mechanisms and the effect that injury has on the tissue.

Although there are many attempts to model the mechanical properties of the brain, it is currently accepted that brain tissue is a non-linear viscoelastic solid with a low strain limit falling between 0.1-0.3%. It has also been agreed that brain tissue is strain-rate sensitive and as strain rate increases, brain tissue becomes stiffer (Franceschini et al., 2006).

2.5 Neck Models and Test Fixtures

Research in the past few decades has investigated modeling concussion test fixtures for the purpose of testing concussion preventative equipment. In this section, we analyze the effectiveness of different neck and head fixtures that have been created in order to leverage a similar design.

2.5.1 Hybrid III

The Hybrid-III test dummy, released by Humanetics Innovative Solutions in 2013, models a 50th percentile male and is used in crash test simulations, as well as for testing the effectiveness of concussion preventive equipment (Shetty & Pan, 2013). The neck and head portion of the Hybrid-III test dummy has been used in a wide range of concussion studies. The Hybrid III neck replicates similar relative mechanical properties to a human neck. The neck is created using alternating rubber and aluminum disks with a cable through the center. The skull is modeled using cast aluminum parts and vinyl skins to cover the skull. The assembly of the components of the Hybrid III neck can be seen below in Figure 3.

Neck Assembly – Harmonized

Figure 3: Hybrid III Neck Assembly (Humanetics Innovative Solutions, 2015)

The Hybrid-III is feasible to replicate and is relatively low cost but is stiffer than the actual human neck as it does not properly imitate the cervical muscles (Eckersley et al., 2019). In Figure 4 we show the static flexion testing results of the Hybrid III. Based on the graph, there is a linear relationship between the applied moment and the angle of bending. The average stiffness value of the Hybrid III neck is 21.70 in-lb/degree or about 2.45 Nm/degree. This is approximately 100 times higher than the neck stiffness values found on humans described in section 2.2.2 and Table 1.
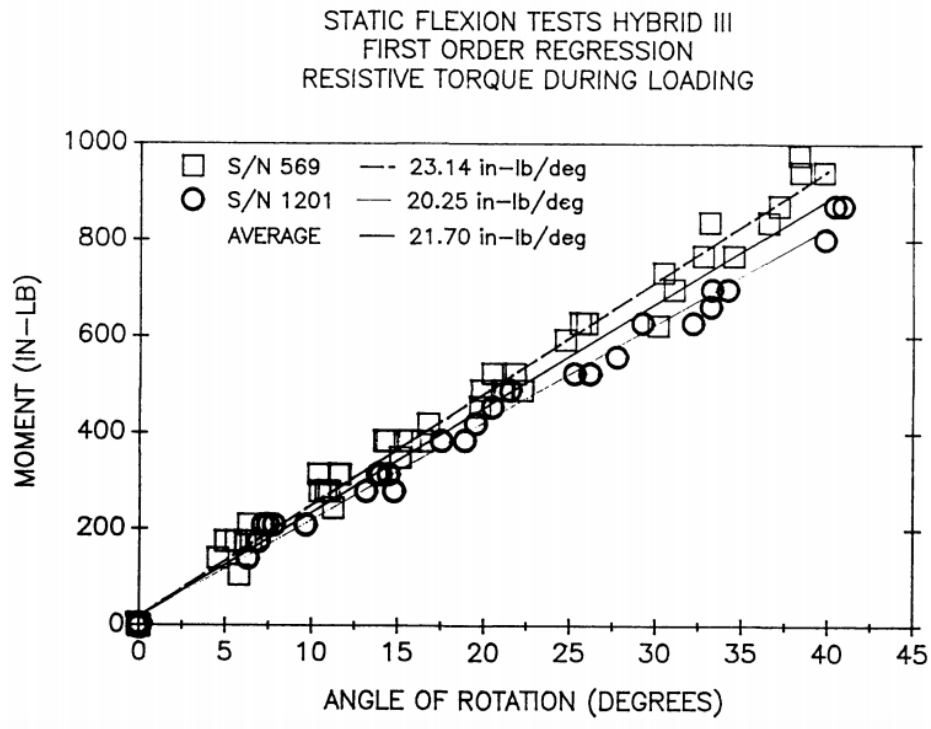
Figure 4: Hybrid III Static Testing Results (Spittle et al., 1992)

2.5.2 Past MQP Projects

Past major qualifying projects (MQPs) at WPI have re-created the Hybrid III neck for testing new concussion gear they designed. The MQP titled "Design and Development of a Football Neck Support and Testing Apparatus" from 2019 constructed their own concussion test fixture and testing rig in order to test the effectiveness of their football neck support design (Merchant et al., 2019).

The neck used for testing was modeled after the Hybrid III neck. The materials used to construct the neck were 3" diameter, ¼" thick aluminum disks, 2 ½" diameter, ¾" thick #30 durometer neoprene, and a 6 strand ½" steel cable that was tensioned to 5.41 ft-lbs. to replicate the strength of a human neck. The choice of these materials was based off a prior

study from 2014 that also re-modeled a Hybrid III neck for testing their concussion gear design (Perry et al., 2014).

The head was made of Styrofoam filled with 8 lbs. of fishing weights to imitate the actual weight of a human head (Merchant et al., 2019). This head deteriorated over an extended period of testing time, so the MQP group recommended that a head could be 3D printed or molded with a more durable material that can be weighted.

In order to simulate an impact to the head, a pendulum was used. To vary the amount of force in the impact, different weights were used, and the pendulum was raised to different heights. This method was chosen instead of using a pneumatic cylinder because the cylinder could not produce a quick enough impact to accurately mimic an NFL football hit (Merchant et al., 2019). In order to avoid multiple impacts on the head from the pendulum, the fixture was placed on sliding rails, with the speed and distance traveled controlled using set screws on the rail sliders.

The previous project's design of the fixture was sufficient for their testing purposes but could be improved upon in future work. The recreated Hybrid III neck fixtures have deteriorated over time and are not long-lasting. It would be beneficial for future studies testing concussion preventive gear to have an accurate head and neck model that is long-lasting.

3.0 Assembly Design

The following section outlines the steps we took in order to accomplish our objectives: (1) Design a test fixture which accurately simulates the relative properties of the human neck and head, (2) Use CAD simulations to determine that the fixture will withstand the force of impact, (3) Test the completed fixture to confirm it accurately models the relative mechanical properties of a human neck, (4) Assess the relationship between neck strength and concussion likelihood. Included in this section are our design constraints, fixture design, and test methods.

3.1 Developing a Design and Constraints

To design our neck and head test fixture, we selected materials with similar material properties to the Hybrid III neck and the human head. The materials we chose influenced our results and the strength of the neck. We also considered the durability of the materials to ensure that this fixture can be reused for future studies. Besides materials, the dimensions of the structure and the overall weight are important. In this section, we identified the design constraints and the materials that resemble the properties of bone, brain tissue, and vertebra in the spine that continue up the back of the neck. We also give reasoning for the size of various parts of the assembly and how we made design decisions.

3.1.1 Modeling the Skull

When choosing a material for the skull, we considered the material properties to ensure that it would withstand testing. It was also important to select a material that somewhat replicated the properties of bone so that forces were accurately transferred throughout the model. Another constraint that heavily influenced our design was that the skull had to be designed such that accelerometers were able to be embedded in it and would remain accessible during testing.

Finally, the skull assembly had to be head shaped so that future teams can test equipment using our fixture.

When modeling the skull, we considered the hardness, elastic modulus, and density of the material we chose (Toro Ibacache, 2013). Table 4 below shows the material properties for various materials with similar mechanical properties as bone taken from CES EduPack.

Table 4: Properties of Bone Mimicking Materials (CES EduPack 2016, 2017)

Material	Young's Modulus (GPa)	Density (kg/m³)	Fracture Toughness (MPa √ m)	Tensile Strength (MPa)	Yield Strength (MPa)
Bone	**~4-18**	**1.4e3**	**3.1 ± 1.8**	**68 ± 18**	**50-190**
Epoxy Resin	3.08	1.16e3	1.85-2.2	55.2-82.7	44.2-66.2
Maple	9.9-12.1	480-590	3.9-4.7	6.18-75.5	43.9-53.7
Pine	9.1-11.2	410-510	3.1-3.7	54.3-66.3	37.1-45.3
Cedar	11.6-14.2	430-530	3.3-4	73.3-89.6	28.8-35.2
PLA	3.3-3.6	1.24e3	3.34-4.79	47-70	55-72

Based on the material properties outlined in Table 4 above, our team used epoxy resin to mold our skull. Although epoxy resin has the lowest Young's modulus and fracture toughness out of the options, it is very similar in density and tensile strength to bone. The other benefit to using epoxy resin is that it is inexpensive and easy to mold. We considered using various types of wood, however, machining the wood to be the correct size would be a challenge given the resources available to us. Furthermore, we were concerned about cracking the wood and the low density given the impact that the head will have to withstand. The material properties of PLA are the closest to bone, however, the 3D printed PLA that is available to us would not have the same properties as solid PLA. Buying solid PLA would not only be expensive, but it would also be nearly impossible to machine to be the correct size given our limitations. Before purchasing the

resin, we used SolidWorks simulations to analyze the stresses on the skull under an impact force of 1700N (largest ever recorded in football) as a worst-case scenario analysis as we do not plan to exceed this value during testing.
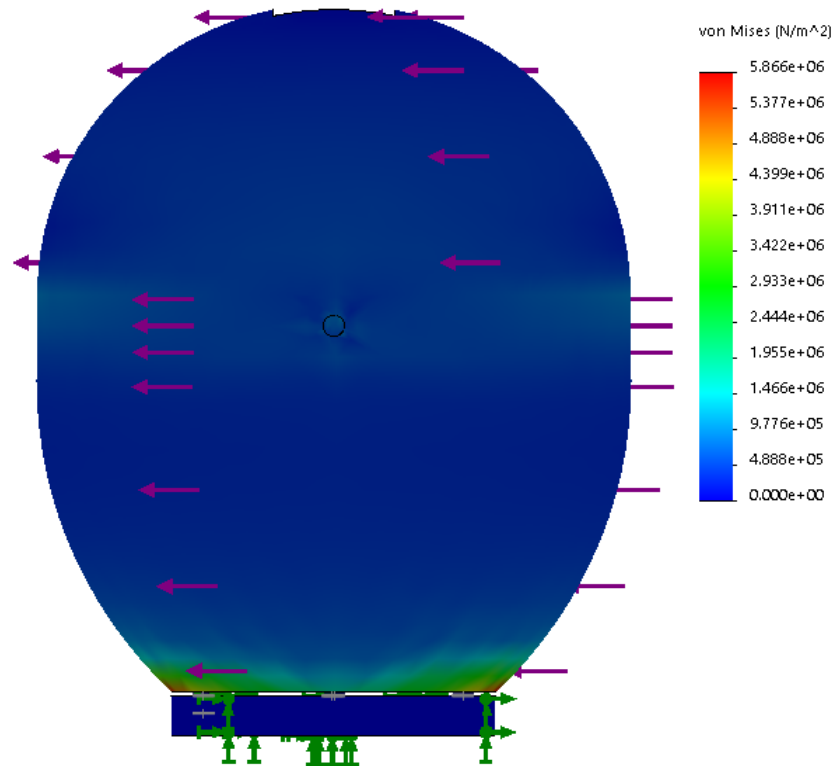
Figure 5: SolidWorks Head Simulation- Deflection: 0.000333m

Based on the SolidWorks simulations of the head, the maximum stresses of 5.86 MPa are located where the screws connect it to the top of the neck. In addition, the deflection was measured at 0.00033 meters. Because the deflection is relatively small and the maximum stress experienced in the head is about 10 times lower than the yield strength of our epoxy resin seen in Table 4 (44.2-66.2 MPa), we knew that it would withstand the force of impact.

After confirming the epoxy resin would be strong enough, we molded the skull in two parts using 3D printed PLA molds, then joined the two resin casts with Velcro and duct tape after they hardened. We molded the top half of the skull to be "bowl" like in shape to allow for a cavity for the brain to sit in. To mold the top half of the skull, we 3D printed a two-part mold that was bowl shaped with a similar diameter to a skull. A concentric Styrofoam piece was suspended inside the 3D printed mold to create the cavity for the brain to sit in. We chose to use Styrofoam because it is cheap and can be easily removed from and suspended in the resin during hardening. After the resin hardened, we demolded the top part and sanded it to get rid of the rough exterior. We then machined accelerometer slots into the resin using a Dremel. Figure 6 below shows the process of molding the skull with epoxy.

| Part A of Epoxy Resin | Mix Part A | Part B of Epoxy Resin |
| Mix Part A and Part B together | Pour resin into 3D printed mold | Place Styrofoam in the mold |

Figure 6: Top Skull Epoxy Molding Process

Originally, we planned to make the bottom half of the head solid; however, after molding the top part and recognizing the weight, we re-designed the bottom half of the skull so that it would use less resin and weigh less. Our redesigned bottom half had a hole through the center of it which allowed for the top of the neck to sit in the bottom of the skull. The hole also acted as an opening to allow the accelerometer wires to pass through to the Arduino. Because the neck had to attach to the bottom part of the skull, we originally planned on drilling screws through the bottom of the resin. However, after consulting with WPI's machine shop and analyzing our simulations, we decided to mold threaded inserts into our resin. To do this, we 3D printed a copy of our top disk to align the inserts properly and submerged them into the wet resin while it cured. For de-molding purposes, the mold was created in two pieces and covered with duct tape and petroleum jelly before the wet resin was poured in.

3.1.2 Modeling the Brain

Identifying a material to model the brain was more difficult than modeling the skull because of its complex anatomy and the variation in test methods that are described in section 2.4.2. Finding a material that modeled the brain was important because it allows for the proper simulation of how the brain would move relative to the skull during a concussive impact. We had to find a material that has similar shear and viscoelastic properties as brain tissue as this would affect the acceleration. Another constraint for the brain material was that it had to be long-lasting and could not degrade after repetitive hits.

Because it has been accepted that brain tissue is viscoelastic, the shear modulus and elastic modulus are time dependent (Finan et al., 2017). Finan et al. attempted to measure the shear modulus of the brain and determined that it is highly variable depending on the length of testing and type of tissue tested. Figure 7 from Finan et al. shows the shear modulus of various kinds of brain tissue as a result of indentation testing over different time intervals.
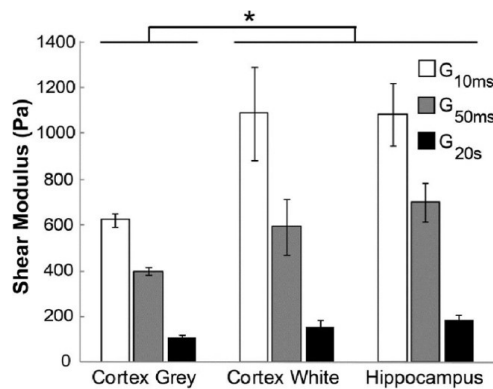
Figure 7: Shear Modulus of Brain Tissue Over Time

Franceschini et al. concluded based on their cyclic uniaxial stress tests, that brain tissue is similar in material properties to filled elastomers or rubber materials (2006). Tan et al. (2018) created a composite hydrogel out of polyvinyl alcohol and phytagel (PVA-PHY) that accurately mimics the viscoelastic properties of brain tissue (2018), however, given our limitations creating this was not possible. Another study by Lozoya (2016) tested various kinds of gelatin and agarose mixtures and found that mixing 3% gelatin with 1% agarose has a similar elastic modulus of brain tissue (2016). Table 5 below summarizes some of these materials and their properties in comparison to brain tissue.

Table 5: Properties of Brain Tissue Mimicking Materials

Material	Young's Modulus (Pa)	Density (kg/m³)	Shear Modulus (Pa)
Brain Tissue	**3,240**	**1,040**	200- 1,300
Silicone	240,000	1,050	103,000
3% Gelatin 1% Agarose	7,900- 29,000	unknown	unknown
Natural Rubber	1,200,000-2,100,000	930-970	400,000-700,000

After researching a variety of materials and consulting with WPI's Professor Songbai Ji, we decided to use silicone to model our brain. While silicone does not precisely match the properties of the human brain, its high durability and flexibility make it the most reasonable material choice (Bilston, 2011). We found silicone to have the most comparable viscoelastic properties to human brain tissues of any long-lasting, non-degradable material. The silicone brain simulant would be able to deform against the skull during impact, with the capability of being repeatedly used for testing. To ensure the brain would fit nicely into the skull, we used the top part of the skull as our mold for the brain. Before pouring the silicone mixture into the head, we covered the head cavity in petroleum jelly for de-molding purposes. Figure 8 below shows the process of molding the silicon brain. The silicone used in the brain was Smooth-On Ecoflex 00-10 which was chosen because of its shore hardness factor. An X-Acto knife was used to cut a slot into the center of the brain to accommodate the accelerometer inserted vertically into the brain.

Mix Part A and Part B together   Pour mix into molded top skull   Let silicon set and dry

Figure 8: Brain Molding Process

3.1.3 Modeling the Neck

The main design constraint considered when designing the neck was that it must accurately replicate the relative strength of human necks and be able to be altered to replicate a variety of different neck strengths. Another constraint we considered was that the materials we choose must be long-lasting so that our fixture can be reused in the future. Finally, the neck had to interface with the other subassemblies.

We engineered a similar model to the Hybrid III because ordering the exact parts of the model were too far out of budget for our purposes. We modeled our neck off the Hybrid III crash test dummy neck based on the success of previous MQP teams with similar designs and the validation testing already done on the design. A picture of the Hybrid III neck assembly is shown in Figure 9 below.

Figure 9: Hybrid III Neck and Head

Like the Hybrid III neck, we used alternating rubber and aluminum disks. Previous MQP teams used durometer neoprene #50 and were successful in modeling the mechanical properties (Perry et al., 2014). To obtain the desired shape of the neoprene disks, we used hole saws and grinded off the blades to give the hole saw a sharp edge. Next, we used the hole saws to press and cut the desired disks out of the neoprene sheets. We machined the three ¼" thick aluminum disks at WPI's machine shop.

Through the center of the rubber and aluminum disks, we designed a tensioning cable, allowing us to alter the neck strength. Originally, we planned to use a similar tensioning cable design as previous MQP teams, however, after seeing the degradation, we chose to get a ½" steel cable professionally manufactured at St. Pierre Wire Rope. To prevent the cable from rotating, we originally developed the design seen below, but based on St. Pierre's capabilities, the final cable came with two cylindrical steel ends swaged on.

Figure 10: Original Steel Cable Rotation Prevention Design

Because the tensioning cable came with two ends already swaged on that were significantly larger in diameter than the ½" steel cable, we had to make the center hole of the aluminum and neoprene disks bigger than we had planned. To account for them wobbling on the tensioning cord, we used a piece of rubber vinyl tubing to fill in the excess space between the

cord and the center holes on all disks. In addition, since the new swaged end was larger than

expected, we had to significantly redesign our top disk so that it would properly interface with

the end of the cable and the resin skull. The top of the neck was machined with a channel to

allow for the cable to slide onto the disk and drop down so the swaged end sits in the disk. Figure

11 below shows our re-designed top disk. We considered using set screws in the top disk to

prevent rotation of the cable, but after assembly we realized this was not necessary because the

cable did not rotate freely. We altered the neck strength by using a torque wrench to turn the

locking nut up/down on the threaded end of the steel cable.

Figure 11: Final Steel Cable Design

3.1.4 Modeling the Torso

There are a few constraints we considered when designing the torso section of our

fixture. First, the torso had to be strong enough to withstand the forces of the pendulum. Second,

the torso had to be heavy enough to accurately simulate a human torso, but it also had to be able

to be disassembled in smaller pieces for easy transportation. Finally, the torso had to properly

interface with the subassemblies.

Based on the constraints outlined above, we decided to build the torso in two sections out of hollow, steel columns and plates. Steel is easy to weld and had the right mechanical and physical properties required to withstand the force of the pendulum. We used SolidWorks simulations using a force of 1700N (maximum ever recorded in football) to ensure that our design would be able to withstand impacts in testing. Based on the simulation, the maximum stress that the torso experiences under a force of 1700N is 27.2 MPa and a deflection of 0.000134m. Because the deflection is very small and the maximum stresses are significantly smaller than the yield strength of steel (241 MPa), we confirmed that the steel torso would not break or undergo any plastic deformation during testing.
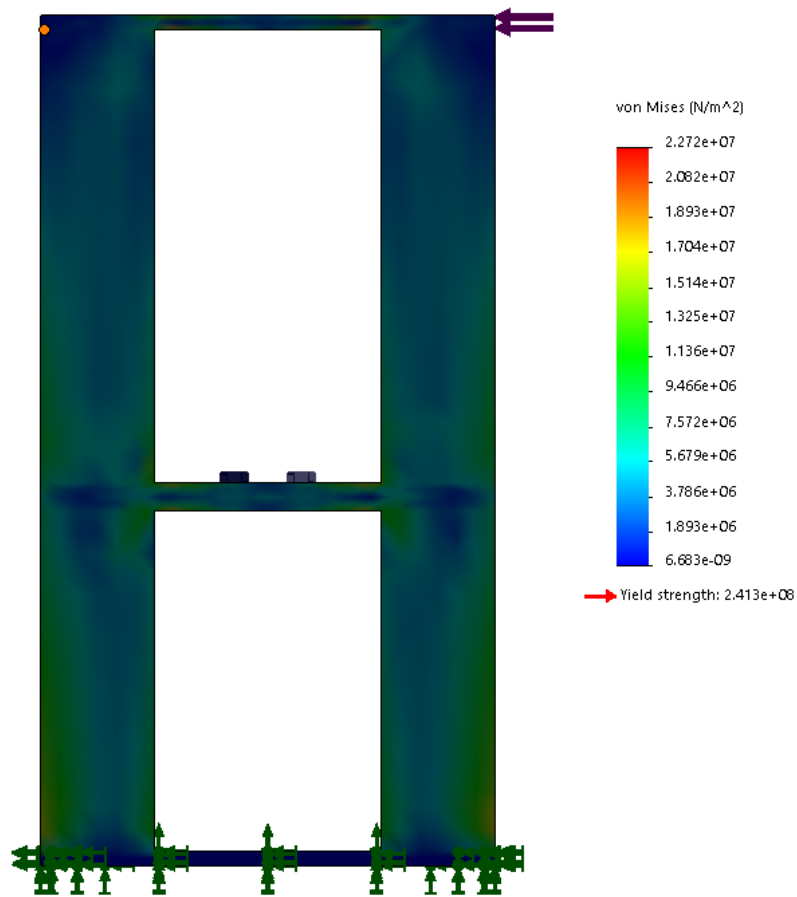
Figure 12: SolidWorks Simulation of the Torso- Deflection: 0.000134m

28

The framework for the torso subassembly includes 2 separate boxes, each one made of two (8" x 8") steel plates of ¼" thickness and 4 (2" x 2.5") square tubes of 0.188" thickness. Originally, we designed the topmost plate to contain a circular array of holes, allowing the head and neck assembly to rotate on top of the torso. However, because our fixture is symmetrical and rotating the head during testing would not produce different results, we decided to secure the bottom disk to the top plate using only four holes.

By building the torso in two separate sections, the assembly may be easily taken apart for transportation and storage convenience. We welded the columns to the corners of the steel plates at WPI's machine shop. We determined the height of the steel columns based on the length of the threaded end swaged onto the cable. Because we wanted to allow for maximum tensioning, we made the columns for the top portion 8" tall. Once the two separate boxes were built, we attached them to one another using nuts and bolts. A model of the torso can be seen in Figure 13 below.

Figure 13: Final Torso Assembly

The swaged ends of the cable also resulted in a design change for the steel plates in the middle of the torso. The center hole that the cable travels through was machined larger to allow the swaged end to fit through it. To allow for tensioning large washers along with a nut were purchased. The nut and washer combination allow for tensioning by preventing the cable from traveling back through the hole in the center plate.

3.2 Final Design and Fixture Assembly

The final assembly of the fixture was performed in the Robot Pits in the WPI Recreational Center. The base of the torso was attached to the sliding plate from a previous MQP using four 5/16"-18 nuts and bolts. There are enough through holes to use 8 nuts and bolts, but for our purposes, only 4 were required. After the bottom of the torso was secured to the sliding plate the plate was placed on the rails and the top of the torso was positioned on the bottom of the torso. Eight 5/16"-18 nuts and bolts were used to secure the two torso sections together. Once the torso was assembled the neck and head could be assembled.

The various disks and tubing were assembled onto the cable. The bottom of the skull was attached to the top disk of the neck using four 5/16"-18 bolts screwed into the inserts and various washers between the two to even out the levelness of the skull. The accelerometer was placed in the brain and connected to the necessary wires needed to collect the axis we needed. The brain was then placed in the top of the skull. The two halves of the skull were attached to each other using duct tape and Velcro, allowing the wires to travel down the center hole of the bottom of the skull and the top of the neck. The entire neck assembly was then placed into the torso assembly and secured using four 5/16"-18 nuts and bolts attaching the top of the torso to the bottom disk of the neck. The nut and washers were then added to the threaded end of the half inch cable to fully

secure the neck to the torso. A torque wrench was used on the neck nut to attain the correct

torque to model the various necks we wanted.

3.2.1 Accelerometer Orientation and Set-Up

Initially, two accelerometers were going to be used to measure the acceleration, one in

the center of the brain and the other embedded on the inside of the back of the skull. Having two

accelerometers, with one in the center of the head and the other on the outside would allow for

the calculation of the angular acceleration of the head. This would be done by assessing the

difference in accelerations at each accelerometer based on the distance between them.

Orienting and fixing the accelerometers within the skull and brain was critical to the

accuracy of our data. To attach the accelerometer into the brain, we used a Dremel to create a

slot for the accelerometer to sit and then used hot glue to attach it. For the accelerometer in the

brain, we cut a vertical slit which we inserted the accelerometer into. The placements and

orientations of the accelerometers in the head can be seen in Figure 14 below.
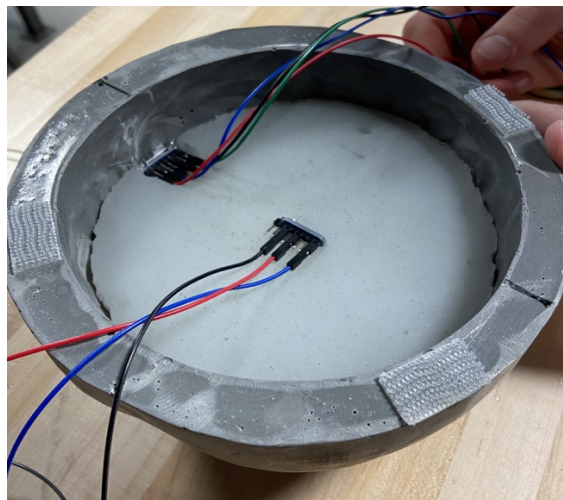
Figure 14: Brain and Head Accelerometer Placements

We took note of the orientation of the accelerometers in order to identify which axes we would be looking to obtain data from. We also cut out a small portion of the brain so that the wires from the accelerometer in the skull were not obstructed by the brain. This also served to make sure that the axes from the two different accelerometers aligned in the same plane.

4.0 Design Validation

After assembling our final fixture, we had to validate that the fixture we created would behave like an impact created in a sports game. To do so, we calculated how much weight to add to the pendulum to achieve our desired force. Furthermore, we conducted static testing to gain an understanding of how neck bending stiffness related to the torque of the tensioning cable. This section explains how we validated our design.

4.1 Pendulum Calculations

In order to apply force to the head to simulate a concussion-causing blow, a pendulum will be used to hit the head. One previous MQP constructed a pendulum to simulate a concussion blow in order to test their football neck support. The idea of using a pneumatic cylinder to apply force was considered, but it could not simulate the necessary speed and force. The pendulum constructed had a total height of 9 feet, and a pendulum arm of 6 feet and 5lbs (Buckley et al., 2019). The original arm from this pendulum was not used. Instead, a new pendulum arm was created with a length of 44 inches and weight of about 3lbs. Weights were added to the pendulum bob in order to change the amount of force applied.

To ensure that the pendulum was hitting our fixture with a force comparable to those seen in sports, we derived an equation relating force of the pendulum to the weight we added to the

bob. In order to do this, we had to use the equations for a physical pendulum and use the basic principle that $\sum \tau = I\alpha$. We considered using the conservation of energy principles to determine the angular velocity at impact, however by using these equations, the mass of the pendulum bob would cancel out as it has no effect on the period of the pendulum.

In our calculations outlined below, we treated the pendulum as a compound pendulum consisting of a rod and a bob. We treated the bob as a point mass because the geometry of it changed as we added different weights. We also assumed an elastic collision between the pendulum and our fixture as an approximation. Because we were only going to be dropping the pendulum from angles less than 30 degrees, we were able to use the small angle approximation formulas. We outline these calculations below, which were later used to determine the ideal drop weight and pendulum angle:

Table 6: Summary of Nomenclature for Pendulum Calculations

Symbol	Units	Meaning
I	lbf*ft*s²	Moment of Inertia
M_B	lb	Mass of Pendulum Bob
M_R	lb	Mass of Pendulum Rod
L_R	Ft	Length of Pendulum Arm
D_B	ft	Distance between pendulum bob and origin of rotation
D_R	ft	Distance between COM of Rod and origin of rotation
R_{CM}	ft	Radius of center of mass
Alpha	Rad/ s²	Angular acceleration of pendulum
F	lbft / s²	Force of impact

Inertia of the Pendulum (Treating pendulum bob as a point mass)

$$I_{Total} = I_R + I_B$$

$$I_{Total} = [\frac{1}{3} M_R (L_R)^2 + M_R (D_R)^2] + [M_B (D_B)^2]$$

$$I_{Total} = [\frac{1}{3} (4)(3.76)^2 + (4)(1.88)^2] + [M_B (3.76)^2]$$

$$I_{Total} = [33] + [14.14 M_B]$$

Radius of Center of Mass

$$I = MR^2$$

$$R_{CM} = \sqrt{\frac{I}{(M_B + M_R)}}$$

$$R_{CM} = \sqrt{\frac{(33 + 14.14 M_B)}{(M_B + 4)}}$$

Angular Acceleration

$$\alpha = \frac{g}{R_{CM}} sin(\theta)$$

$$\alpha = \frac{32.2}{\sqrt{\frac{(33 + 14.14 M_B)}{(M_B + 4)}}} sin(30)$$

$$\alpha = \frac{16.1}{\sqrt{\frac{(33 + 14.14 M_B)}{(M_B + 4)}}}$$

Force of Impact Relating to Mass of Pendulum Bob

$$F = \frac{I\alpha}{R_{CM}}$$

$$F = \frac{(33 + 14.14 M_B) * [\frac{16.1}{\sqrt{\frac{(33 + 14.14 M_B)}{(M_B + 4)}}}]}{\sqrt{\frac{(33 + 14.14 M_B)}{(M_B + 4)}}}$$

$$\boldsymbol{F\ [lbf] = 16.1(M_B + 4)}$$

$$\boldsymbol{F\ [N] = 4.45 * F\ [lbf]}$$

4.2 Static Testing

After building our fixture, we calculated neck stiffness values through static testing to compare the values to a real human neck and the Hybrid III. In addition, we created a graph that shows the relationship between the neck stiffness values and the torque values to which we tensioned the cable. Since our neck model does not have active muscles to provide strength, we assumed that the stiffness of our neck model correlates to the relative strength of a human neck. The tensioning cable allowed us to alter the stiffness of our neck model which we used as a measure of human neck strength in our testing.

4.2.1 Procedure

To test the static neck stiffness values in relation to the torque of the tensioning cable, we laid our completed fixture sideways on a lab bench. We removed the epoxy resin head to allow us to easily attach weights to the top disk of the neck assembly. Next, we tensioned the neck to the minimum value and hung known masses from the end of our neck. By using a piece of string attached to the end of a ruler, we were able to measure the vertical displacement of the neck as seen in Figure 15.

Figure 15: Static Neck Testing Set-Up

We calculated theta by taking the inverse tangent of the vertical displacement divided by the total length of our neck and converting to degrees. Finally, we were able to calculate the bending stiffness (in Nm/degree) of our neck by dividing the torque induced by the hanging mass (Nm) divided by the angular displacement (degrees). The detailed calculations can be found in section 4.2.2. We repeated this procedure for varying torque values while keeping the hanging mass constant.

4.2.2 Results and Calculations

To calculate the neck stiffness values in Nm/degree, we treated the neck as a cantilevered beam. To do so, we measured the vertical displacement (Δ) and solved for the angle of bending (θ) using the inverse tangent. Next, we divided the torque induced by the hanging mass by the change in angle. We show the equations we used to calculate these below:

Calculating k in Nm/deg

$$k \left[\frac{Nm}{deg} \right] = \frac{mgL}{\theta}$$

We compiled our static testing data into Table 7 below. In addition, we graphed the torque wrench values vs. the stiffness values to determine the relationship between them. We used this trendline equation in section 6.1 to convert the torque wrench settings into neck stiffness values. Figure 16 shows the graphical relationship between torque and neck stiffness (k) as a result of our static testing.

Table 7: Static Testing Data

Torque Wrench Setting (Nm)	Hanging Mass (kg)	Δ (m)	θ (Degrees)	k (Nm/deg)
3.6	9.07	0.019	7.36	1.77
4.5	9.07	0.022	8.51	1.54
5.3	9.07	0.018	6.98	1.87
6.2	9.07	0.019	7.36	1.77
6.7	9.07	0.016	6.21	2.10
7	9.07	0.012	4.67	2.79
8	9.07	0.011	4.28	3.05
8.7	9.07	0.012	4.67	2.80
9.5	9.07	0.0095	3.70	3.53
10.4	9.07	0.0099	3.85	3.39
11.3	9.07	0.0085	3.31	3.95
12.1	9.07	0.008	3.12	4.19
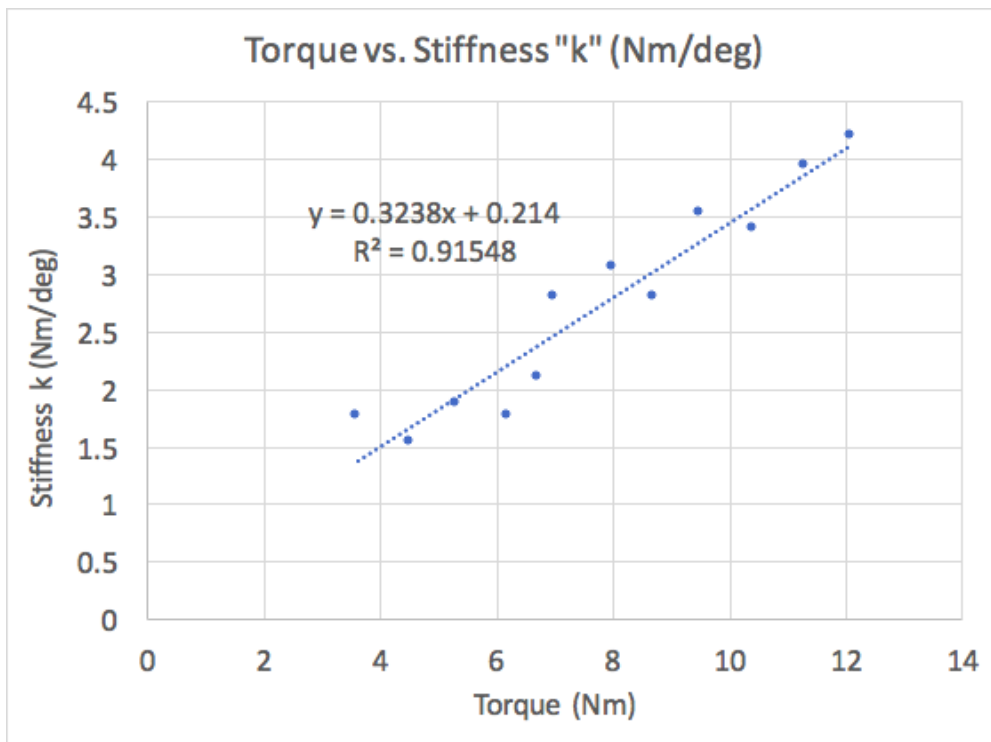
Figure 16: Torque vs. Stiffness "k" in Nm/degree

4.2.3 Analysis

Based on the graphs above, we concluded that there is a linear relationship between the torque we set the tensioning cable to and neck stiffness. In Figure 16, the correlation coefficient for a linear regression was greater than 0.9 indicating a good linear fit. Based on our background research, male necks are about 1.5 times stronger than female necks (Catenaccio et al., 2017). The relationship between strength, stiffness, and torque allowed us to select torque values to simulate the difference between male and female necks.

With this data, we were able to compare our neck fixture to the Hybrid 3's properties. We also compared our neck fixture's strength to the strength of a human neck. Based on column 7 in Table 7 above, our stiffness values ranged from 1.77 to 4.19 Nm/deg. The Hybrid 3 static testing showed a similar bending stiffness of 2.45 Nm/deg as described in section 2.5.1 of the Background. In contrast, the measured stiffness for human necks is only in the 0.01-0.30 Nm/deg range depending on the angle of bending. Because of this, we concluded that our neck fixture is approximately 200 times stronger than a human neck, even at the lowest torque setting.

5.0 Testing

After building our fixture and validating the properties of it, we began assembling the fixture with the pendulum to prepare for testing. In this section, we outline our test method and the way we collected and interpreted data.

5.1 Test Rig Set-up

The shorter pendulum rod resulted in the pendulum bob not making contact with the head when placed on the ground. To accommodate for the reduced length, we placed the sliding rails on a folding table. The increased height of the table allowed for the pendulum to contact the center of the head. Once the rails were properly aligned with the pendulum, duct tape was placed at the end of the rails and along the side of the rails to allow for repeatable alignment during sequential tests. We show our experimental set-up below.


Figure 17: Fixture and Pendulum Experimental Set-Up

Initially we planned on taking data from two accelerometers at the same time. Both accelerometers would take measurements from two axes to calculate the angular acceleration of the head for the HIP equation. However, after confirming that the HIP equation was not relevant as our head could not move relative to the neck, we proceeded with only measuring accelerations from one accelerometer. In addition, after initial testing with our two-accelerometer configuration, we determined that the sampling rate of 600 Hz was too low to gather enough data points during the 15-millisecond time interval used in the HIC equation. Through testing, we confirmed that the sampling rate for one accelerometer measuring two axes was around 1200 Hz, which doubled the sampling rate compared to when we were taking measurements from two accelerometers. As a result, we conducted our tests using only one accelerometer located in the center of the brain.

5.2 Testing Procedure

When identifying the ideal conditions for dropping the pendulum, we were looking to achieve a hit that had both high impact and was repeatable. Previous MQP reports mentioned that the pendulum motion was not repeatable for angles larger than 30 degrees. In order to set the drop angle to 30 degrees, we used trigonometry to determine the horizontal distance (22 in) that the pendulum should be pulled back to from the resting position. During testing, the same person measured the horizontal distance and another person dropped the pendulum to ensure the most accurate repeatability. Between each trial, the nut at the end of the steel cable was checked and adjusted to the proper torque to account for any loosening during impact. In order to further enhance repeatability of testing, we wanted to make sure that the sliding rails and fixture were in the same position for each hit. In order to accomplish this, we placed duct tape on the folding

table outlining the starting position of the sliding rails. In between each test, we readjusted the torque setting on the neck and lined up the sliding rails along the duct tape.

In order to determine the weight to use during testing, we conducted 10 trials each for pendulum weight of 35 pounds and 50 pounds and a pendulum angle of 30 degrees, as outlined below in Section 5.5. Our results showed that trials with 35 pounds were significantly more repeatable than trials with 50 pounds. As a result, 35 pounds is what we chose to be our ideal drop conditions for our main testing.

5.3 Data Collection

Initially, we planned to use LabVIEW and a data acquisition system in order to collect data. We decided to switch to an Arduino board setup after realizing how bulky and immobile the data acquisition system was. The Arduino system was easy to transport, easy to setup, and provided an adequate sampling rate for our testing. Our data acquisition system consisted of an Adafruit ADXL377 accelerometer rated for ±200 g and an Arduino Mega board. To wire the accelerometers, we followed simple wiring instructions available on the Adafruit website after soldering the pins to the printed circuit boards via holes. We also used the coding instructions online to create our code. In order to maximize sampling rate of our system, we removed all portions of the code that were not essential to data collection (See Appendix A for Arduino code and wiring). Once the wiring and code were set up, we would release the pendulum and begin collecting accelerometer readings. After the impact, we copy and pasted the timestamps and raw acceleration data printed from the code into an Excel sheet to be processed.

5.4 Data Evaluation

In order to evaluate the data that was collected, the raw data from the accelerometer (in bits) needed to be converted to the actual acceleration (in g's). First, we had to calibrate the accelerometer readings by subtracting the "at rest" reading (in bits) from all readings. Next, we used the calibration value in mV/g from the AXDL377 specifications to convert the bit values to acceleration values in g's. These calculations can be found in Appendix B.

After all acceleration values were adjusted, we had to find the range of 15 milliseconds that resulted in the highest acceleration. This is because HIC values are typically evaluated over time intervals of less than or equal to 15 milliseconds. Based on our sampling rate of 1200Hz, we knew that 18 data points corresponded to a time range of 15 milliseconds. We then used Excel to calculate the summation of all sets of 18 consecutive data points. The 18 data points that had the sum were the points we used to calculate HIC.

The next step was to calculate the area under the acceleration curve of these 18 data points. This was completed by using a trapezoidal Riemann sum approximation in Excel. After the area under the curve was calculated, we used the HIC equation (described in section 2.1.4) to calculate the HIC value for that trial.

5.5 Testing for Repeatability and Analysis

In order to determine that our experimental test method and set-up was repeatable across various trials, we ran 3 different tests simulating a small impact, medium impact and large impact on the same neck torque value of 3.6 Nm. To simulate different impacts, we changed the weight added to the pendulum bob as well as the drop angle (never exceeding 30 degrees). For

each test, we ran 10 trials and analyzed the average HIC value, the standard deviation, and the coefficient of variation. The summary of these results are shown in Table 8 below.

Table 8: Summary of Test Method Repeatability Trials

Weight added to Pendulum	Drop Angle	Pendulum Force (N)	Average HIC	Standard Deviation	Coefficient of Variation
35 lbs	15 Degrees	190	2.038	0.175	0.086
35 lbs	30 Degrees	360	13.047	1.43	0.11
50 lbs	30 Degrees	400	14.127	4.29	0.30

Based on Table 8 above, we concluded that our test method was repeatable for our purposes. The standard deviations across all trials were relatively low and the average HIC values increased with increased impact force as predicted. Based on our results, we decided to use 35 lbs on the pendulum bob with a 30 degree drop height for our testing. Although a 15 degree drop height yielded a smaller coefficient of variation, we would have had to add more weight to the pendulum bob to get the desired impact force which would have made testing more challenging.

For the chosen testing conditions of 35 lbs on the pendulum bob with a 30 degree drop angle, we were also hoping to see that each hit would have a relatively repeatable graphical output. To assess this repeatability, we looked at the x-axis and y-axis graphs for each of the 10 repeatability test trials conducted. We were looking for visual abnormalities in the graphs to better understand the motion of the head during impact. Figures 18 and 19, below, show the x-axis acceleration of the first two trials conducted. We observed that each of the 10 hits produced very similar graphical results to these figures. Each hit quickly spikes to approximately 15g and then quickly decreases in acceleration. Prior to bouncing back in the opposite direction of the hit (when acceleration becomes negative), there is always a small timeframe of sustained motion at

a relatively low acceleration. Since all hits followed a similar acceleration pattern, we further concluded that our test setup was repeatable.
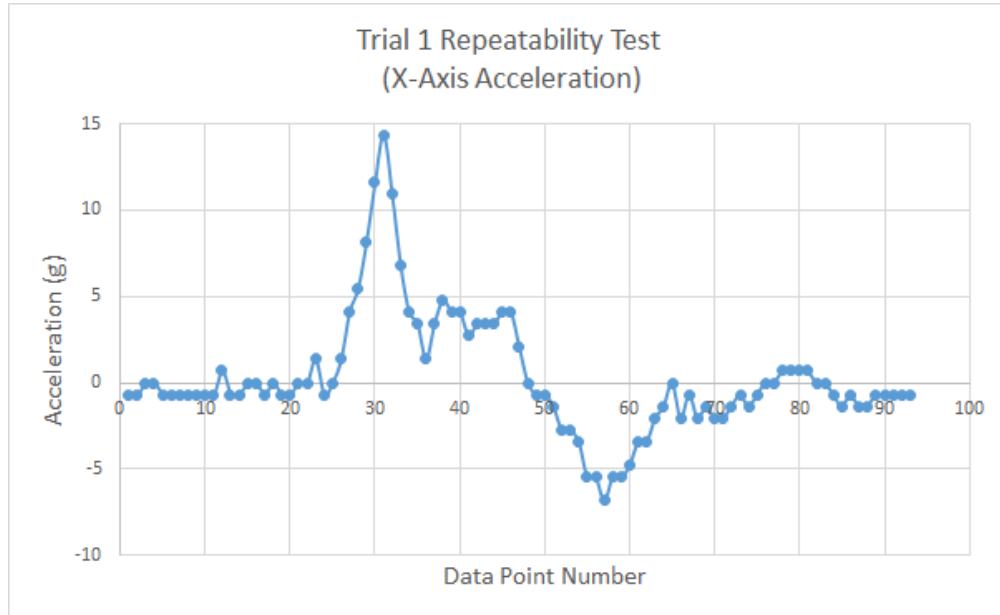


Figure 18: Trial 1 Repeatability Graph- X-Axis Acceleration
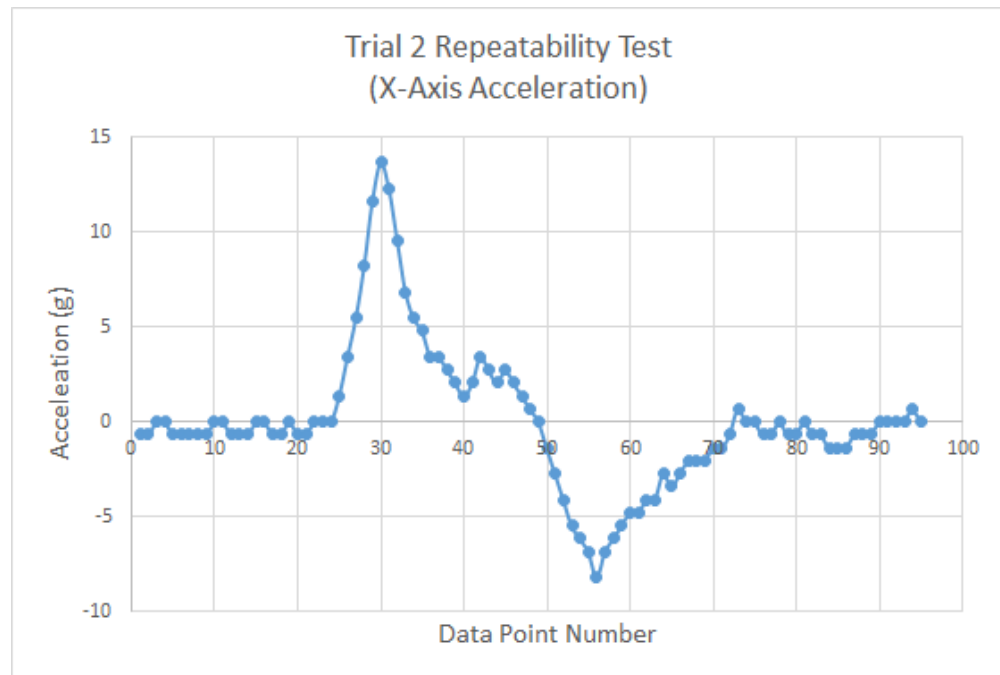
Figure 19: Trial 2 Repeatability Graph- X-Axis Acceleration

5.6 Neck Strength vs. HIC Testing/ Trials

Following the validation of repeatability of our test conditions, we were prepared to collect our data. Since our neck was considerably stiffer than a human neck, we wanted to assess the relationship between neck strength and HIC by using a wide range of stiffness settings. We decided to test the neck with stiffness measures between 1.38 and 3.39 Nm/deg (this corresponded to the maximum and minimum range available with our torque wrench). We divided this range of stiffness into 7 equal settings. We took 10 trials for each stiffness value resulting in a total of 70 data points, which resulted in a noticeable relationship between the strength of a neck and the HIC measures. Appendix C shows the raw data taken from the accelerometers during two of the trials from our testing. Appendix D contains the excel sheet formulas used to calculate the results from this raw data. A table of the calculated data obtained from all 70 trials can be found in Appendix E.

6.0 Results and Discussion

Existing research has suggested that an increase in neck strength is likely to decrease the risk of concussion likelihood. A study completed by Collins et al. (2014) evaluated the impact of neck strength on concussion prevalence in 6,662 athletes. The results showed that athletes who had sustained a diagnosed concussion had a mean neck strength of 8.04 pounds (35.6 N), compared to 9.54 pounds (42.4 N) for uninjured athletes. In fact, when the data was adjusted for gender and sport, for every pound of additional neck strength, the concussion risk decreased by 5 percent. A different study involving NFL athletes provided further evidence that neck strength is an important factor in reducing rotational acceleration of the head that causes concussions.

While these studies provide evidence that neck strength is an important factor in preventing concussions, they rely solely on injury diagnosis and mathematical modeling. We physically modelled these parameters by creating a test fixture with variable simulated neck strength. This allowed us to assess the relationship between neck strength and acceleration of the head during impact. Our hypothesis was that by increasing simulated neck strength of our fixture, the resulting acceleration of the head would decrease.

6.1 Neck Strength vs. HIC Values

After conducting 70 data tests, we found a strong relationship between simulated neck strength of our fixture and HIC values. Figure 20, below, is a set of box and whisker plots for each of the 7 different neck stiffness values we tested. Table 9 below shows the torque wrench setting, the stiffness (calculated using the static testing data trendline in Figure 16), and the resulting HIC averages. Finally, Figure 21 displays the average HIC value for each stiffness setting and the trendline explaining their relationship.

Table 9: Calculated Neck Stiffness vs. HIC Values

Torque Wrench Setting (Nm)	Calculated Neck Stiffness (Nm/deg)	Average HIC Value
3.61	1.38	8.95
4.24	1.59	7.14
5.00	1.83	7.78
5.96	2.14	6.86
7.00	2.48	6.12
8.25	2.89	7.32
9.81	3.39	6.13
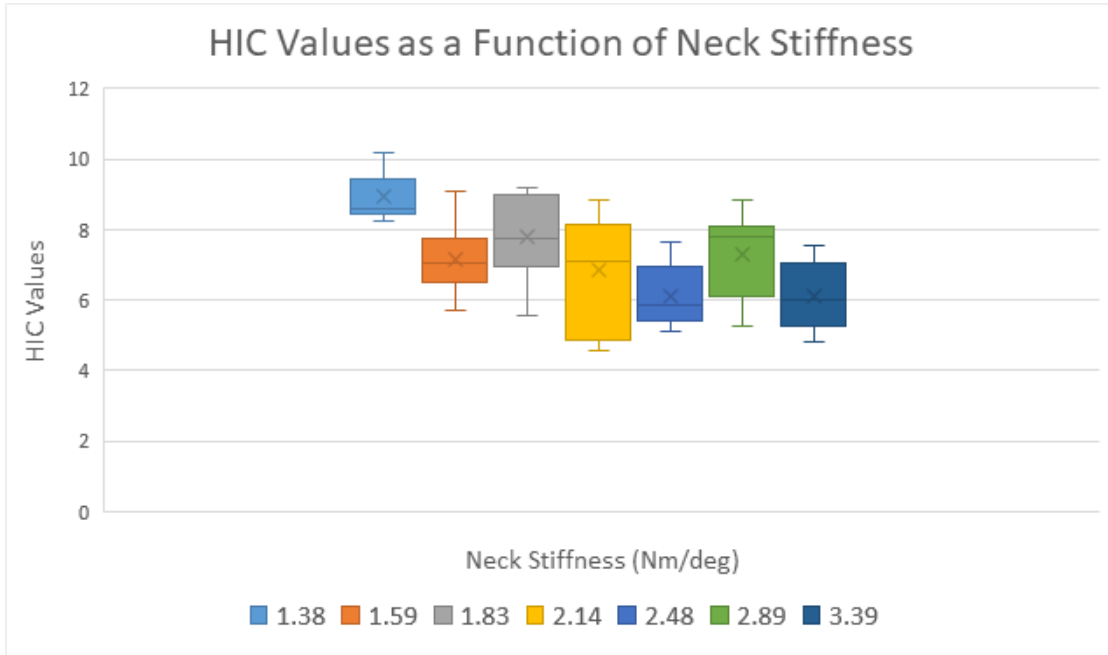
Figure 20: HIC Values vs. Neck Stiffness- Box and Whisker
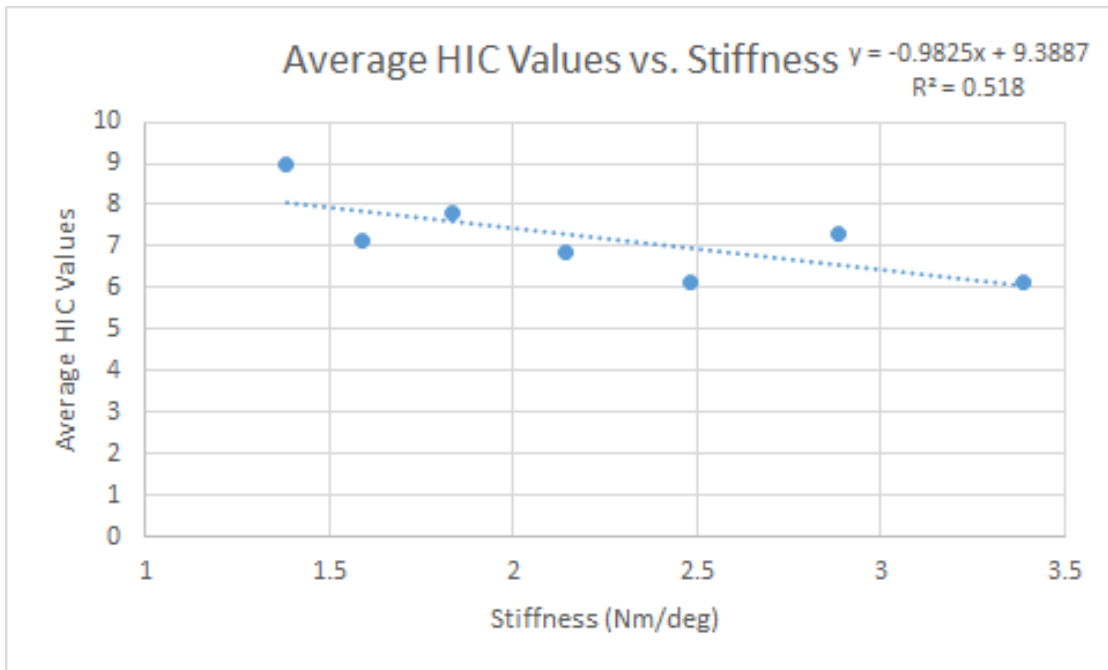
Figure 21: HIC Values vs. Neck Stiffness- Scatter Plot Trendline

Our evidence supports our hypothesis that increasing neck strength decreases concussion likelihood. Males have a neck strength about 1.5 times greater than females (Catenaccio et al., 2017). Based on our data, as neck strength is increased by a factor of about 1.5, the resultant HIC values decrease by approximately 5.9 percent. This calculation was completed by using the trendline associated with all 70 data points, as shown in Figure 21. The data from our physical model provides evidence to support the claim that females are more likely to sustain concussions given the same impact conditions, partially due to the differences in neck strength between males and females.

6.2 Neck Strength vs. Maximum Acceleration Values

Along with assessing the relationship between simulated neck strength and HIC values, we also assessed the relationship between neck strength and acceleration of the head. Figure 22, below, is a box and whisker plot that shows peak resultant acceleration of the head as a function of the 7 different neck stiffness values that were tested. Once again, the data shows a clear downward trendline (as seen in Figure 23) that indicates as simulated neck strength increases, the acceleration of the head decreases. Since maximum acceleration of the head is another injury metric that is frequently evaluated, the data supports our hypothesis that increasing neck strength decreases concussion prevalence.
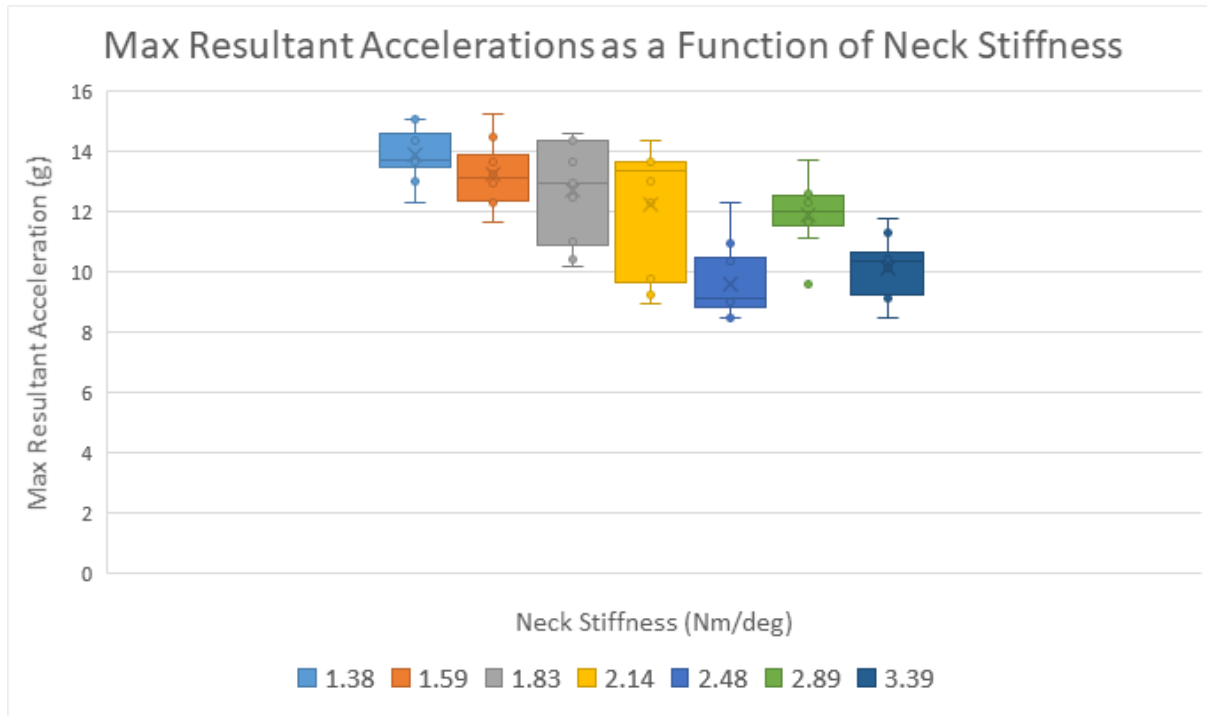
Figure 22: Resultant Acceleration vs. Neck Stiffness- Box and Whisker
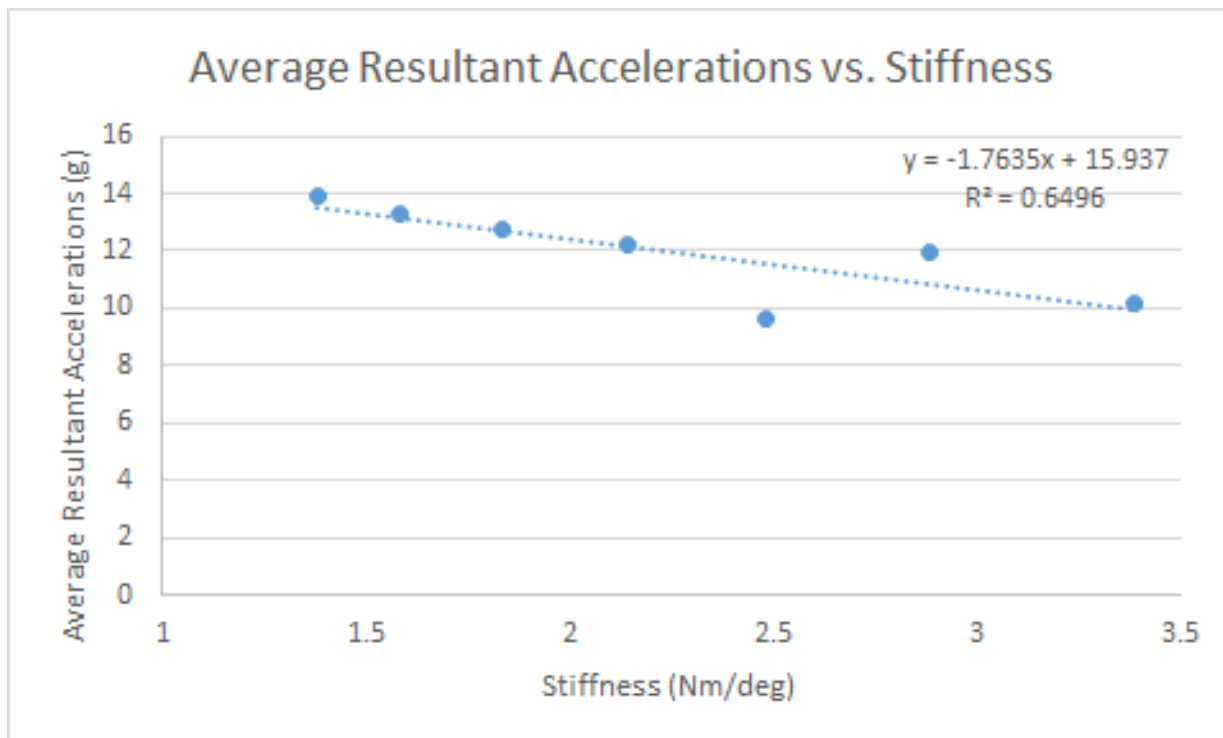
Figure 23: Resultant Accelerations vs. Neck Stiffness- Scatter Plot Trendline

6.3 Extrapolation to Human Neck

While the data provided in this discussion suggests that increasing neck strength decreases concussion likelihood, it is important to note that the physical model created does not exactly match the actual properties of a human neck. As we confirmed through static testing and calculations in section 4.2, our neck fixture was significantly stiffer than a human neck, even at the lowest torque setting. While we were able to create a stiffness vs. acceleration linear fit, extrapolating that data out to the actual stiffness of a human neck may not be accurate given our fixture was about 100 times stiffer. To determine what kind of accelerations we would obtain with a human, we performed the following calculations outlined below:

Table 10: Summary of Nomenclature for Extrapolation to Human Neck Calculations

Symbol	Units	Meaning
I	0.305 Kgm^2	Moment of Inertia of Neck/Head (see Appendix F for calculation)
τ	Nm	Torque
F	360 N	Force of Pendulum (from pendulum calculations, section 4.1) for 35 lb pendulum bob, 30 degree drop
α	Rad/ s^2	Angular Acceleration
θ	Radians	Angle of Rotation
m	5 kg	Mass of Head (5kg)
k	Nm/rad	Neck Stiffness
R	0.147 m	Length of Neck (0.147)
x	m	Horizontal Displacement
t	0.015 s	Time duration of impact

First, it was important to compare the displacement for a neck with low stiffness vs. high stiffness values. In order to calculate the maximum horizontal displacement of the neck after an impact, we used the concept that acceleration is the second derivative of displacement. In the sample calculations below, we use our data from the 10 trials where our neck was set at the lowest stiffness, simulating a female neck (torque wrench set at 3.61 Nm, stiffness: 1.38 Nm/deg seen in Table 11). To calculate the HIC values for these trials, we took the integral of the

50

measured linear acceleration over a 15 ms time interval using a Reimann sum approximation. The Reimann sum approximations of the acceleration values for these trials ranged between 0.18 m/s and 0.20 m/s. In the calculations below we used the average value of about 0.19 m/s. This integral corresponded to the average velocity of the head after the impact with the pendulum. Integrating this value again over a 15 ms time interval gave us the total displacement.

Calculating Displacement

$$x = \iint a(t)dt$$

$$x = \int 0.19\, dt$$

$$x = 0.19 * t$$

$$x = 0.19 * 0.015$$

$$x = 0.0029\, m$$

Once we calculated the horizontal displacement of the head during impact, we were able to calculate the angle of rotation of the head and neck using geometry. Because our head was so stiff and not able to rotate more than 30 degrees, we used the small angle approximation formula outlined below.

Calculating Theta (small angle approximation)

$$\theta = \frac{x}{R} = \frac{0.0029}{0.147} = 0.019\, rad = 1.09°$$

Next, we were able to use the angle of rotation that we found and Newton's second law to relate this value to acceleration. Newton's second law states that force equals mass multiplied by linear acceleration. When talking about angular acceleration, Newton's second law converts to $\sum \tau = I\alpha$. To sum the torques, we had to subtract the resisting torque of our neck (which we treated as a spring: $k\theta$) from the overall torque that the pendulum induced on the head ($F * R$). In this case, I corresponds to the total inertia of the head which we calculated to be 0.305 kgm^2 using the parallel axis theorem (see Appendix F). Because the weight and dimensions of our head were like a human, we assumed that the inertia of a human head would remain the same.

Angular Acceleration and Torque

$$T = I\alpha$$

$$F * R - k\theta = I\alpha$$

$$360 * 0.147 - k\theta = 0.305\alpha$$

$$\alpha = \frac{-k\theta + 52.9}{0.305}$$

By using the equations above, we concluded that the accelerations a person experiences after a hit is related to the stiffness of their neck and the angle that their head rotated. By using our data and background research, we were able to substitute in varying stiffness (k) values and their corresponding angle of bending (θ) after an impact to compare the resulting accelerations that we calculated theoretically. Table 11 below summarizes the angle of bending, stiffness values, and resulting accelerations for various models. Because we were not able to measure the

angle of bending for an actual human, we used the maximum range of motion of a male and

female neck which are about 70 degrees and 80 degrees respectively (Youdas et al., 1992).

Table 11: Extrapolation Calculations to Compare Acceleration for Various Models

Title	Torque Wrench Value (Nm)	Neck Stiffness (k Nm/deg)	Neck Stiffness (k Nm/rad)	Measured Angle of Bending (θ radians)	Acceleration (α rad/s^2)
Fixture Simulating Female Neck	3.61	1.38	79.1	0.019	169
Fixture Simulating Male Neck	5.96	2.14	122.68	0.016	167
Human Female Neck	N/A	0.01	0.573	1.40	171
Human Male Neck	N/A	0.03	1.72	1.22	167

Based on Table 11, it seems that neck stiffness and the degree of bending do not have a

large effect on the overall head acceleration under a constant force of 360 N. The calculations

above show that the impact from the pendulum or magnitude of the hit has a larger effect on the

angular acceleration of the head than the neck strength does. Although quantitatively this model

does not necessarily support our findings, qualitatively it makes sense. The final equation that we

derived shows that acceleration is negatively correlated with stiffness, thus as stiffness increases,

acceleration decreases. This finding supports our hypothesis and data that we collected.

There are a few reasons why this model is quantitatively inaccurate. The model suggests

that the collision between the pendulum and head is fully elastic. This assumption ignores that

the force decreases throughout the duration of collision. Realistically, the force being transferred

to the head is a function of time. As the force decreases over time and is transferred to the head, the deflection of the head increases until all the force has been transferred. As this occurs, we would observe varying acceleration values rather than the average acceleration values we calculated in Table 11. In addition, this model neglects damping. In the physical system, there would be oscillations due to the spring properties of the neck. However, in our calculations we neglect these frequencies. Finally, our fixture and calculations were not able to simulate the difference between active vs. passive neck stiffness. When a person sustains a blind impact, they do not have time to flex their neck muscles and therefore, passive stiffness of the neck becomes relevant. In the equations above, we are purely looking at the varying stiffnesses and corresponding theta values that we measured. Depending on if it was a blind hit or not, the theta values would vary drastically based on our background research.

6.4 Sources of Error

While we had done tests to ensure the repeatability of the hits and accelerometer readings, there was still variance between the same tests which can be attributed to many different factors. The pendulum arm was pulled back by one of our team members, while another measured the appropriate distance between the head and the pendulum bob. While the same members were conducting the tests each time, and the same distance was measured, there could have been human error in these tests. The person holding the pendulum could have moved the position of the pendulum arm very slightly before dropping it. The measurement was done with a tape measure that does not have extremely precise tick marks on it, so the distance could have slightly varied for each test.

After each test, the rails moved by the force of the pendulum hitting it, so it needed to be realigned each time. We placed tape on the table to align the rails, but the alignment was done by eyeballing the placement of the rails in relation to the tape. Therefore, the rails may not have been in the exact same location for each test. Throughout the testing, the sliding rails progressively lost more ball bearings. This could have changed the rate at which the fixture slid back after a hit.

Lastly, the accelerometer and Arduino may have been a source of error. The measurements read from the accelerometer would sometimes oscillate between different values when at zero acceleration. This was likely due to faulty wire connections that were moved from all the impacts to the head. Furthermore, the Arduino Mega only had sampling rates up to 1200 Hz when measuring two axes on one accelerometer. Because of this, we were only able to record 18 data points highlighting each impact. Having more data points during the impact may have made our trials more repeatable by better capturing data from the impact.

7.0 Recommendations

Due to these sources of error and limitations of our study, we make some recommendations for future studies below:

- Add a force sensor to the pendulum or on the head where the pendulum strikes it to measure exactly how much force is being subjected to the head for each test to ensure repeatability.

- Use smaller steel tubes for the torso to make accessing the nut to tension the cable easier.

- Put middle disks on the cable before swaging on the ends of the cable.

- Do not use a 3D printed mold for the top disk when molding the bottom of the head because it deformed from the heat when molding the epoxy resulting in uneven placement of the threaded inserts.

- Get a good mold release and use a mold that will not leak (leaked through cracks of 3D printed molds screwed together). Possibly use a putty on the crack to prevent leaking rather than duct tape.

- Add an auto-release mechanism to pendulum to ensure the same release and height each time.

- Creating own wires for accelerometer to Arduino to allow for easier connections.

- Higher sampling rate from the accelerometer – write to file instead of using the print function

- Put accelerometers in locations that are easier to wire. The accelerometer in the skull could have been on the outside of the skull.

8.0 Conclusions

Over the recent years, there has been significant research to understand the reason why female athletes are much more likely to be diagnosed with concussions than their male counterparts in the same sports. One suggested possibility to explain this phenomenon is the difference in neck strength between male and females. This idea has been studied using diagnosis history of athletes and various mathematical models, but there is little documentation on physical models that test this hypothesis. Despite our limitations, we were able to design a fixture and collect data suggesting that a difference in neck strength affects the likelihood of a concussion. Based on the 70 trials in our experiments, as neck strength increases, the HIC and peak acceleration values of the head decrease under an impact of 360 newtons. This magnitude of force is something that one might observe in a soccer collision. While more data points should be obtained in order to more accurately assess this relationship, our physical model provides evidence to support this claim. Based on the data collected using our test fixture, HIC values are 5.9 percent higher for females than males given the same impact conditions.

9.0 Appendices

Appendix A: Arduino Code and Wiring

```
// X is red, Y is blue, Z is orange, Vin is green, Ground is black

// Pins for First Accelerometer (Brain)
// +x Backward, -x Forward
// +y Up, -y Down
const int x_brain = A0;
const int y_brain = A1;
int x_brain_val;
int y_brain_val;

// Pins for Second Accelerometer (Skull)
// +y Up, -y Down
// +z Forward, -z Backward
// const int y_skull = A8;
// const int z_skull = A9;
// int y_skull_val;
// int z_skull_val;

void setup() {
  Serial.begin(115200);
}

void loop() {

  // Read Accelerometer 1
  x_brain_val = analogRead(x_brain);
  y_brain_val = analogRead(y_brain);
```

```
// Read Accelerometer
// y_skull_val = analogRead(y_skull);
// z_skull_val = analogRead(z_skull);


// Print to Serial as Test (**comment out to increase sampling rate**)
Serial.println("\t" + String(x_brain_val) + "\t"+ String(y_brain_val));
// +"\t"+ String(y_skull_val) + "\t"+ String(z_skull_val));


}
```
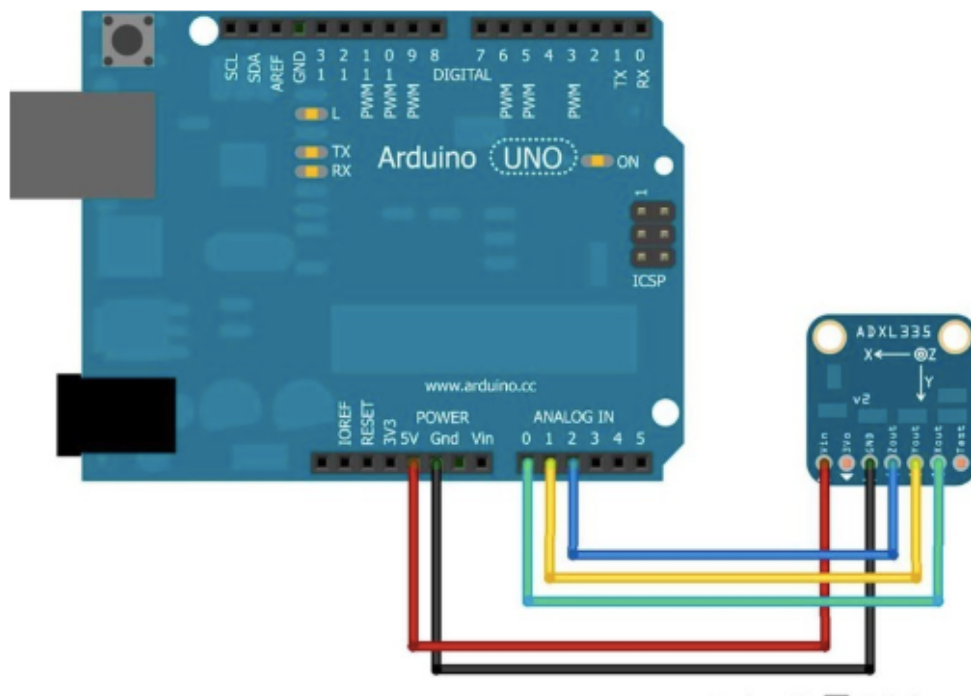

Figure 24: Adafruit Tutorial Arduino Wiring Set-Up

Appendix B: Converting Accelerometer Bytes to Acceleration Values (g's)

In order to read the data from the accelerometer through the Arduino, we needed to calibrate the accelerometer. The following calculations were done in Excel after taking the Arduino readings from each trial and converting the bytes to acceleration values. The Arduino outputs data in bytes, so this needed to be converted from bytes to voltages to accelerations. The accelerometer has a zero-g reading of 1.5V based on the AXDL377 data sheets. The equation below converts the bytes read by the Arduino to voltages.

$$Voltage\ (V) = Accelerometer\ reading\ (bytes) * \frac{1.5V}{zero\ g\ reading\ (bytes)}$$

The accelerometer value is the reading displayed by the Arduino for a given instant. The zero g reading is the reading displayed by the Arduino when the accelerometer is at zero acceleration. This zero g reading was taken during the same trial as when the impact occurred, but from before the actual impact when the fixture was not moving.

Once the voltages were calculated from the byte readings, they then needed to be converted to acceleration values. The ADXL377 accelerometer data sheet gives a mV to g rating of 6.5mV/g. This can be used to convert the voltage values to accelerations in g's.

$$acceleration\ (g) = \frac{Voltage(V) - 1.5(V)}{0.065\ (\frac{V}{g})}$$

Appendix C: Raw Accelerometer Testing Data
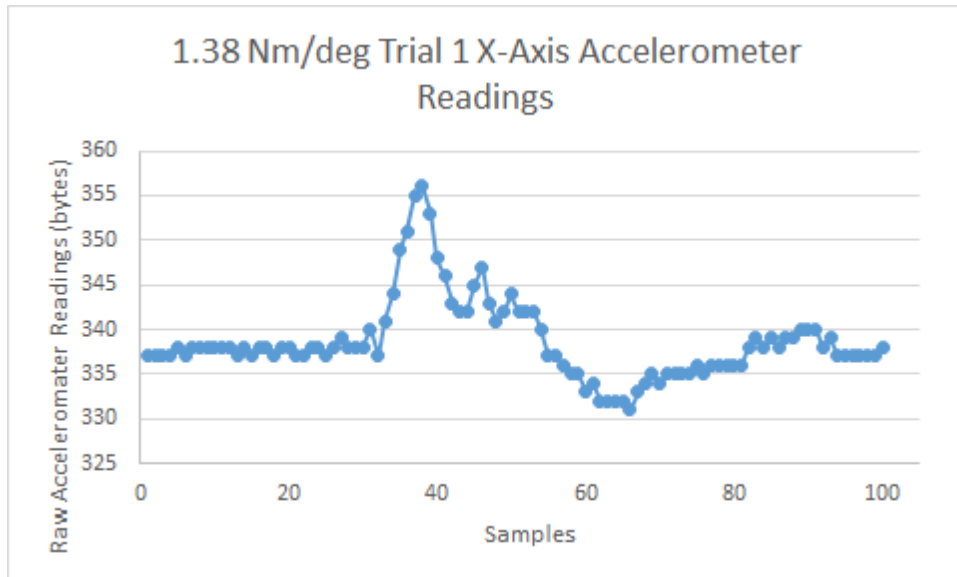
Figure 25: 1.38 Nm/deg Trial 1 X-Axis Accelerometer Readings
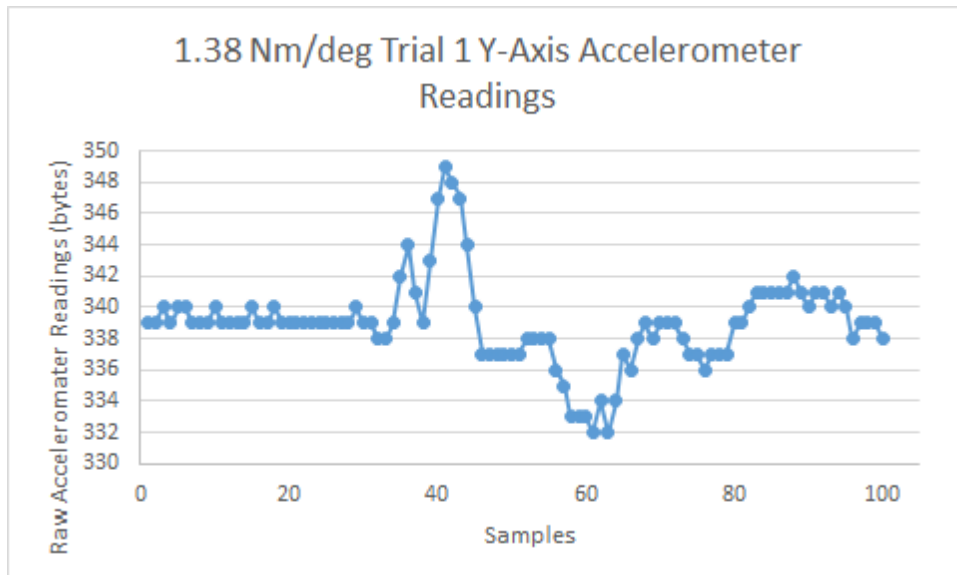
Figure 26: 1.38 Nm/deg Trial 1 Y-Axis Accelerometer Readings
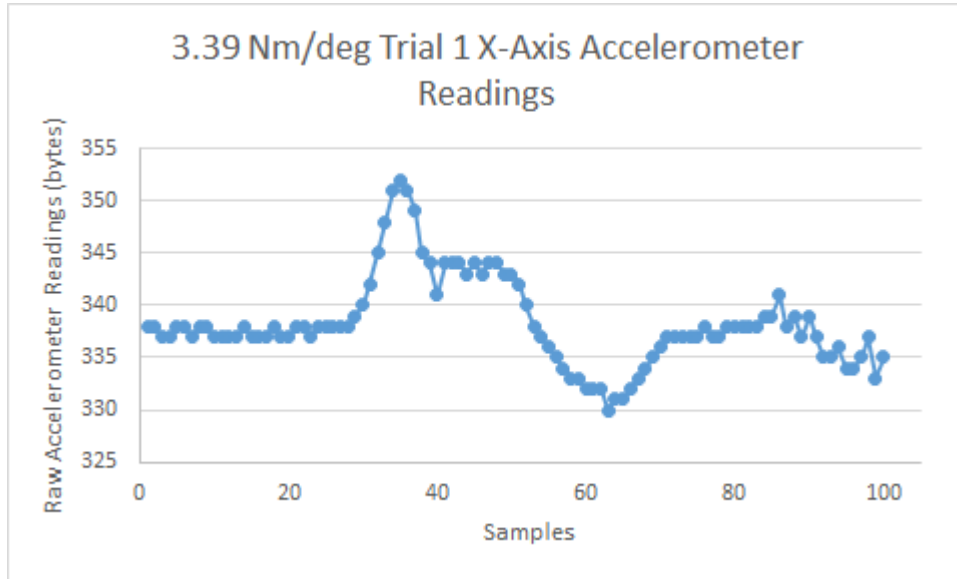
Figure 27: 3.39 Nm/deg Trial 1 X-Axis Accelerometer Readings
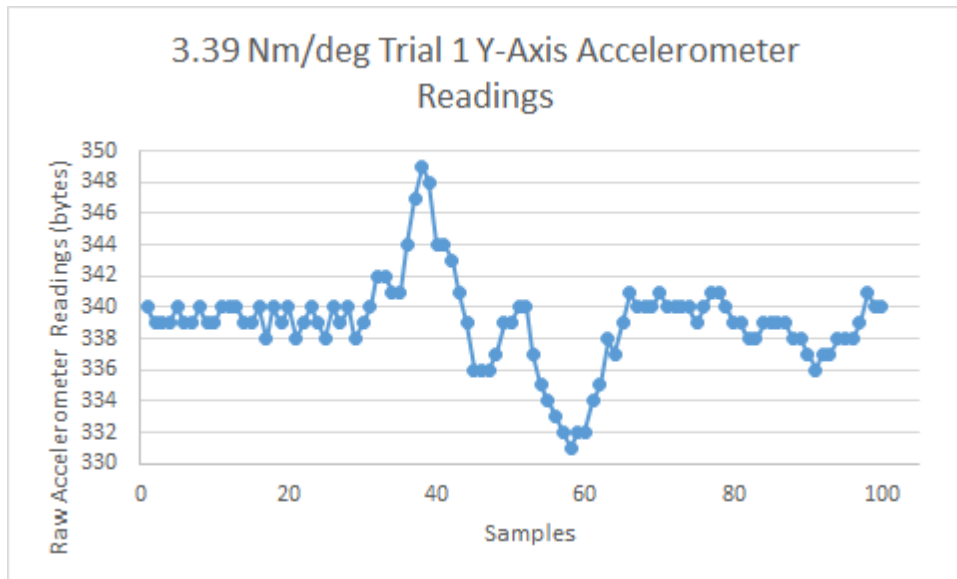
Figure 28: 3.39 Nm/deg Trial 1 Y-Axis Accelerometer Readings

Appendix D: Excel Formulas Used to Calculate HIC

Table 12: Excel Formulas for Converting Raw Data to HIC Values

Raw X Accelerometer Readings	A_{XR}
Raw Y Accelerometer Readings	A_{YR}
Zero g X Accelerometer Reading	A_{X0}
Zero g Y Accelerometer Reading	A_{Y0}
Number of Samples Collected	s
Calibrated X in g's	$$A_{XC} = \frac{1.5 \times (\frac{A_{XR}}{A_{X0}} - 1)}{0.0065}$$
Calibrated Y in g's	$$A_{YC} = \frac{1.5 \times (\frac{A_{YR}}{A_{Y0}} - 1)}{0.0065}$$
Sum of Calibrated X	$$\Sigma_{XC} = \sum_{n=s}^{18} A_{XC}$$ Sum of 18 consecutive points
Sum of Calibrated Y	$$\Sigma_{YC} = \sum_{n=s}^{18} A_{YC}$$ Sum of 18 consecutive data points
Max of Calibrated X Sums	$M_X = MAX(\Sigma_{XC})$ Take the 18 data points that contributed to the max of the sums.
Max of Calibrated Y Sums	$M_Y = MAX(\Sigma_{YC})$ Take the 18 data points that contributed to the max of the sums.
Resultant Accelerations	$$A_R = \sqrt[2]{A_{XC}^2 + A_{YC}^2}$$ The corresponding calibrated X and Y values in g's for the 18 data points are used to find the resultant accelerations.
Riemann Sum	$$R = \frac{(A_{R_n} + A_{R_{n+1}})}{2} \times 0.0015$$
Integral of 18 Data Points	$$I = \sum_{n=s}^{18} R$$
HIC	$$(\frac{I}{0.015})^{2.5} \times 0.015$$

	A	B	C	D	E	F	G	H	I	J	K	L	M	N
1	Timestam	Raw X	Raw Y	Calibrated X	Calibrated Y	SUM	SUM	MAX	BRAIN ACC		Resultant	Reiman Sur	Integral	HIC
699	13:12:04.7	338	338	0.68477517	-0.6807352	78.06437	36.07897	100.6619	5.478201	2.042206	5.846477	0.0102382	0.180573	7.542129
700	13:12:04.7	338	340	0.68477517	0.68073519	82.17302	39.48264	40.16338	7.532527	2.042206	7.804458	0.0131156		
701	13:12:04.7	338	339	0.68477517	0	86.28167	40.16338		9.586852	1.36147	9.683044	0.0150334		
702	13:12:04.7	338	340	0.68477517	0.68073519	89.70555	40.16338		10.27163	1.36147	10.36146	0.015401		
703	13:12:04.7	339	338	1.36955033	-0.6807352	93.8142	37.44044		9.586852	3.403676	10.17314	0.0150234		
704	13:12:04.7	340	339	2.0543255	0	96.5533	36.07897		8.217302	5.445882	9.858077	0.013947		
705	13:12:04.7	342	340	3.42387583	0.68073519	99.2924	34.03676		5.478201	6.807352	8.73789	0.0123876		
706	13:12:04.7	345	342	5.47820132	2.04220558	100.6619	31.99455		4.793426	6.126617	7.77897	0.0091109		
707	13:12:04.7	348	342	7.53252682	2.04220558	99.2924	29.95235		2.739101	3.403676	4.368945	0.0076859		
708	13:12:04.7	351	341	9.58685232	1.36147039	95.86852	27.91014		4.793426	3.403676	5.878941	0.0085438		
709	13:12:04.7	352	341	10.2716275	1.36147039	89.70555	27.22941		4.793426	2.722941	5.512834	0.0078719		

Figure 29: Excel Values and Conversions

Appendix E: Calculated Testing Data

Table 13: HIC and Maximum Accelerations for all Trials

Trial #	Torque (Nm/deg)	Stiffness (k),(Nm/deg)	HIC Value	Max Resultant Acceleration
1	3.61	1.38	9.24	13.01
2	3.61	1.38	10.20	15.08
3	3.61	1.38	8.64	12.34
4	3.61	1.38	8.46	13.70
5	3.61	1.38	10.10	15.08
6	3.61	1.38	9.14	14.40
7	3.61	1.38	8.24	13.65
8	3.61	1.38	8.59	13.72
9	3.61	1.38	8.46	13.65
10	3.61	1.38	8.41	14.48
11	4.24	1.59	7.11	12.99
12	4.24	1.59	9.11	15.27
13	4.24	1.59	6.97	12.99
14	4.24	1.59	7.77	14.48
15	4.24	1.59	7.75	13.72
16	4.24	1.59	5.71	12.36
17	4.24	1.59	6.23	11.69
18	4.24	1.59	6.93	13.25
19	4.24	1.59	7.22	13.65
20	4.24	1.59	6.63	12.31
21	5.00	1.83	7.46	12.97
22	5.00	1.83	5.57	10.44
23	5.00	1.83	6.45	10.17
24	5.00	1.83	8.46	13.01
25	5.00	1.83	9.21	14.64
26	5.00	1.83	9.05	14.40
27	5.00	1.83	7.46	13.70
28	5.00	1.83	7.15	11.04
29	5.00	1.83	8.97	14.44
30	5.00	1.83	8.04	12.49
31	5.96	2.14	8.62	13.76
32	5.96	2.14	7.61	13.67
33	5.96	2.14	7.16	13.67
34	5.96	2.14	4.91	9.28
35	5.96	2.14	4.83	9.77
36	5.96	2.14	4.58	8.98
37	5.96	2.14	7.99	14.35
38	5.96	2.14	7.01	13.04
39	5.96	2.14	6.99	12.31

40	5.96	2.14	8.85	13.67
41	7.00	2.48	7.64	12.34
42	7.00	2.48	7.46	10.98
43	7.00	2.48	6.79	10.36
44	7.00	2.48	5.48	9.13
45	7.00	2.48	5.85	9.01
46	7.00	2.48	5.09	9.01
47	7.00	2.48	5.24	8.47
48	7.00	2.48	5.83	9.13
49	7.00	2.48	5.91	9.13
50	7.00	2.48	5.87	8.47
51	8.25	2.89	8.48	13.71
52	8.25	2.89	7.96	12.40
53	8.25	2.89	7.92	12.62
54	8.25	2.89	6.32	11.69
55	8.25	2.89	7.96	12.34
56	8.25	2.89	5.54	11.69
57	8.25	2.89	5.28	9.58
58	8.25	2.89	7.15	11.15
59	8.25	2.89	8.85	12.49
60	8.25	2.89	7.70	11.66
61	9.81	3.39	7.54	10.36
62	9.81	3.39	5.63	10.44
63	9.81	3.39	5.11	10.15
64	9.81	3.39	4.79	9.28
65	9.81	3.39	6.64	11.79
66	9.81	3.39	6.95	11.29
67	9.81	3.39	7.30	10.36
68	9.81	3.39	6.13	10.36
69	9.81	3.39	5.35	8.47
70	9.81	3.39	5.88	9.13

Appendix F: Calculations for Inertia of Head

Table 14: Nomenclature for Inertia of Head Calculations

Diameter of steel cable	d
Mass of head	m
Total length from bottom end of cable to the center of the head	l
Radius of spherical head	R

$$I_{total} = I_{cable} + I_{head}$$

$$I_{cable} = \frac{\pi}{64} d^4 = \frac{\pi}{64} (0.0127)^4 = 1.27 \cdot 10^{-9} \, Kg \cdot m^2$$

$$I_{head} = I_{sphere} + ml^2$$

$$I_{sphere} = \frac{2mR^2}{5} = \frac{2(5)(0.093)^2}{5} = 0.0173 Kg \cdot m^2$$

$$I_{head} = 0.0173 + ml^2 = 0.0173 + 5(0.24^2) = 0.305 \, Kg \cdot m^2$$

$$I_{total} = I_{cable} + I_{head} = 1.27 \cdot 10^{-9} + 0.305 = \mathbf{0.305 \, Kg \cdot m^2}$$

10.0 References

Bilston, L.E. (2011). Brain Tissue Mechanical Properties. *Biomechanics of the Brain*. 69-89.

    doi: 10.1007/978-1-4419-9997-9_4

Buckley, E. C. F., Hoops, G. P., Cabello, J. A., & Carlton, T. J. (2019). *Design of a Shoulder Pad to Reduce the Risk of Injury in Men's Lacrosse*. *Design of a Shoulder Pad to Reduce the Risk of Injury in Men's Lacrosse*. Worcester, MA: Worcester Polytechnic Institute.

Caccese, J. B., Buckley, T. A., Tierney, R. T., Rose, W. C., Glutting, J. J., & Kaminski, T. W. (2017). Sex and age differences in head acceleration during purposeful soccer heading. *Research in Sports Medicine*, *26*(1), 64–74. doi: 10.1080/15438627.2017.1393756

Catenaccio, E., Mu, W., Kaplan, A., Fleysher, R., Kim, N., Bachrach, T., Lipton, M. L. (2017). Characterization of Neck Strength in Healthy Young Adults. *Pm&r*, *9*(9), 884–891. doi: 10.1016/j.pmrj.2017.01.005

Chancellor, S. E., Franz, E. S., Minaeva, O. V., & Goldstein, L. E. (2019). Pathophysiology of Concussion. *Seminars in Pediatric Neurology*, *30*, 14–25. Retrieved from https://www-sciencedirect-com.ezproxy.wpi.edu/science/article/pii/S1071909119300129

Collins, C. L., Fletcher, E. N., Fields, S. K., Kluchurosky, L., Rohrkemper, M. K., Comstock, R. D., and Cantu, R. C., 2014, "Neck Strength: A Protective Factor Reducing Risk for Concussion in High School Sports," J. Primary Prevent, pp. 309-319

Daneshvar, D. H., Baugh, C. M., Nowinski, C. J., McKee, A. C., Stern, R. A., & Cantu, R. C.

(2011). Helmets and mouth guards: the role of personal equipment in preventing

sport-related concussions. *Clinics in sports medicine*, *30*(1), 145–x.

doi:10.1016/j.csm.2010.09.006

Eckersley, C. P., Nightingale, R. W., Luck, J. F., & Bass, C. R. (2019). The role of cervical

muscles in mitigating concussion. *Journal of Science and Medicine in Sport*, *22*(6), 667–

671. doi: https://doi.org/10.1016/j.jsams.2019.01.009

Finan, J. D., Sundaresh, S. N., Elkin, B. S., McKhann, G. M., Morrison, B., (2017).

Regional mechanical properties of human brain tissue for computational models of

traumatic brain injury. *Acta Biomaterialia*, 55(1). pp. 333-339. doi:

10.1016/j.actbio.2017.03.037.

Franceschini, G., Bigoni, D., Regitnig, P., et al. (2006). Brain tissue deforms similarly to filled

elastomers and follows consolidation theory. *Journal of the Mechanics and Physics of*

Solids. 54(1). 2592–2620. doi: 10.1016/j.jmps.2006.05.004

Granta. (2017). *CES EduPack 2016* [Windows]. Cambridge.

Humanetics Innovative Solutions, Inc. (2015). *Hybrid-III 50th Male Dummy 78051-218-H*

FMVSS208, 49CFR Part 572, Subpart E. Farmington Hills, MI: Humanetics Innovative

Solutions.

Johnson, G. S. (2014). Gray Matter and White Matter in the Brain. Retrieved from

https://braininjuryhelp.com/gray-matter-and-white-matter-in-brain/

Liao, S., Lynall, R. C., & Mihalik, J. P. (2016). The Effect of Head Impact Location on Day of

Diagnosed Concussion in College Football. *Medicine & Science in Sports & Exercise*,

48(7), 1239–1243. doi: 10.1249/MSS.0000000000000896

Littleton, A., & Guskiewicz, K. (2013). Current concepts in sport concussion management: A

multifaceted approach. *Journal of Sport and Health Science*, *2*(4), 227–235. doi:

10.1016/j.jshs.2013.04.003

Lozoya, M. N., (2016). Development of a Tissue-Mimicking Brain Phantom for Neurosurgical

Pre-Operative Planning and Training. *Clemson University All Theses*. Retrieved

from:

https://pdfs.semanticscholar.org/1270/a80b1563ea3c696170414f272c757b837b1b.pdf

Marjoux, D., Baumgartner, D., Deck, C., & Willinger, R. (2006). Head Injury Prediction

Capability of the HIC, HIP, SIMon and ULP Criteria, 143–157. Retrieved from

http://www.ircobi.org/wordpress/downloads/irc0111/2006/Session2/26.pdf

McElhaney, J.H., Fogle, J. L., Melvin, J. W., Haynes, R. R., Roberts, V. L., Alem, N. M.

(1970). Mechanical properties of cranial bone. *Journal of Biomechanics,* 3(5), 495-511.

doi:10.1016/0021-9290(70)90059-X.

McGill, S. M., Jones, K., Bennett, G., & Bishop, P. J. (1994). Passive stiffness of the human

neck in flexion, extension, and lateral bending. *Clinical Biomechanics*, *9*(3), 193–198.

doi: 10.1016/0268-0033(94)90021-3

Merchant, B. P., Saunders, C. R., Lubega, F. P., Gillis, S. P., & Bellion, Z. T. (2019). *Design and Development of a Football Neck Support and Testing Apparatus*. Worcester, MA: Worcester Polytechnic Institute.

Motherway, J.A., Verschueren, P., Perre, G.V., Sloten, J.V., & Gilchrist, M.D. (2010). The Mechanical Properties Cranial Bone. doi: 10.1007/978-3-642-14515-5_197

Nazarian, M.R. Begley & F.W. Zok (2015) A concept for mitigating head injury under translational blunt impact. *International Journal of Crashworthiness, 20:5*, 483-494, doi: 10.1080/13588265.2015.1038866

Pellman, E. J., Viano, D. C., Tucker, A. M., & Casson, I. R. (2003). Concussion in Professional Football: Location and Direction of Helmet Impacts - Part 2. *Neurosurgery*, *53*(6), 1328 1341. doi: 10.1227/01.NEU.0000093499.20604.21

Perry, E. J., Pensing, M. L., Rookey, R. A., Hanna, T. S., & Hunnings, Z. K. (2014). *Design of a Protective Device for Head and Neck Injuries in Football*. Worcester, MA: Worcester Polytechnic Institute.

Rice University. (2013). Bone Structure. Retrieved from https://opentextbc.ca/anatomyandphysiology/chapter/6-3-bone-structure/

Rowson, S., Bland, M. L., Campolettano, E. T., Press, J. N., Rowson, B., Smith, J. A., Duma, S. M. (2016). Biomechanical Perspectives on Concussion in Sport. *Sports medicine and arthroscopy review*, *24*(3), 100–107. doi:10.1097/JSA.0000000000000121

Shetty, S., & Pan, L. (2013). Hybrid III 50th v.8 Official Release. Retrieved from

https://www.humaneticsatd.com/about-us/press-releases/hybrid-iii-50th-v8-official-

release

Spittle, E. K., Shipley, B. W., & Kaleps, I. (1992). Hybrid II and Hybrid III Dummy Neck

Properties for Computer Modelling. *VULNERABILITY ASSESSMENT BRANCH*

BIODYNAMICS & BIOCOMMUNICATIONS DIVISION CREW SYSTEMS

DIRECTORATE WRIGHT-PATTERSON AFB, OH 45433-6573. Retrieved from

https://apps.dtic.mil/dtic/tr/fulltext/u2/a255544.pdf

Tan, Z., Dini, D., Baena, F. R., & Forte, A. E. (2018). Composite hydrogel: A high fidelity soft

tissue mimic for surgery. *Materials & Design,* 160(2), 886-894.

doi: 10.1016/j.matdes.2018.10.018.

Toro Ibacache, M.V. (2013). A finite element study of the human cranium; The impact of

morphological variation on biting performance. *Hull New York Medical School*. 17-20.

UPMC. (2019). Concussion Statistics and Facts: UPMC: Pittsburgh. Retrieved from

https://www.upmc.com/services/sports-medicine/services/concussion/facts-statistics

Youmans, H. (2018). Understanding the Risks for Concussions in Soccer. Retrieved

from https://www.orlandohealth.com/content-hub/understanding-the-risks-for-

concussions-in-soccer

Van Dommelen, J., Hrapko, M., Peters, G. (2009). Mechanical Properties of Brain Tissue:

Characterisation and Constitutive Modelling. doi: 10.1007/978-1-4020-8716-5_12.

Viano D.C. (2005) Head Impact Biomechanics in Sport. In: Gilchrist M.D. (eds) IUTAM

Symposium on Impact Biomechanics: From Fundamental Insights to Applications.

Solid Mechanics and Its Applications, vol 124. Springer, Dordrecht

Wood, T. A., Morrison, S., & Sosnoff, J. J. (2019). The Role of Neck Musculature in Traumatic

Brain Injuries in Older Adults: Implications From Sports Medicine. *Frontiers in*

medicine, *6*, 53.

Youdas, J. W., Garrett, T. R., Suman, V. J., Bogard, C. L., Hallman, H. O., & Carey, J. R.

(1992). Normal Range of Motion of the Cervical Spine: An Initial Goniometric

Study. *Physical Therapy*, *72*(11), 770–780. doi: 10.1093/ptj/72.11.770

Zhang, A. L., Sing, D. C., Rugg, C. M., Feeley, B. T., & Senter, C. (2016). The Rise of

Concussions in the Adolescent Population. *Orthopaedic Journal of Sports Medicine*,

4(8). doi: 10.1177/2325967116662458